Targeting OCA-B/Pou2af1 blocks type-1 diabetes and reduces infiltration of activated, islet-reactive T cells

Heejoo Kim[1,2], Jelena Perovanovic[1,2], Arvind Shakya[1,2,¶], Zuolian Shen[1,2], Cody N. German[1,2], Andrea Ibarra[1,2], Jillian L. Jafek[1,2], Nai-Pin Lin[3], Brian D. Evavold[1], Danny H.-C. Chou[3], Peter E. Jensen[1], Xiao He[1], and Dean Tantin[1,2,*]

[1]Department of Pathology, University of Utah School of Medicine, Salt Lake City, UT 84112, U.S.A.
[2]Huntsman Cancer Institute, University of Utah School of Medicine, Salt Lake City, UT 84112, U.S.A.
[3]Department of Biochemistry, University of Utah School of Medicine, Salt Lake City, UT 84112, U.S.A.

[*]Corresponding authors: Dean Tantin, Department of Pathology, University of Utah School of Medicine, Salt Lake City, UT 84112. E-mail address: dean.tantin@path.utah.edu

[¶]Current address: Celgene, Inc., San Diego, CA 92121

Running title: OCA-B in T1D

Manuscript data:
Characters in title (including spaces): 108
Words in abstract: 262
Character count (including spaces): 80,467
Total main figures: 7
Total main tables: 0

Abstract

Autoimmune therapies aim to inhibit autoreactivity while preserving normal immune function. The transcriptional coregulator OCA-B, also known as Bob.1/OBF-1 (gene symbol *Pou2af1*) is induced in stimulated naïve CD4$^+$ T cells, where it docks with transcription factor Oct1 to regulate genes such as *Il2* and *Ifng*. OCA-B promotes expression of these targets in cases of repeated antigen exposure, a necessary feature of autoimmunity. Polymorphisms in *Ocab* itself and binding sites for Oct1/OCA-B complexes are associated with multiple forms of autoimmunity including autoimmune (type-1) diabetes. We hypothesized that T cell-specific OCA-B deletion would protect mice from type-1 diabetes, and that pharmacologic OCA-B inhibition would provide similar protection. We developed an *Ocab* conditional allele and backcrossed it onto a diabetes-prone NOD/ShiLtJ strain background. T cell-specific OCA-B loss protected mice from spontaneous T1D. Protection was associated with reduced pancreatic T cell and macrophage infiltration and reduced proinflammatory cytokine expression. We profiled prediabetic pancreatic lymph nodes and islets by single-cell RNA sequencing and T cell receptor clonotype analysis. Although lymph nodes showed minimal differences, in the islets CD8$^+$ T cell specificities associated with diabetes pathogenesis failed to emerge in OCA-B deficient activated/memory cells. In contrast, CD4$^+$ clones associated with diabetes were present, but only in anergic cells. The protective effect of OCA-B loss was diminished, or even eliminated, using monoclonal models with high affinity to artificial or neoantigens. Rationally-designed membrane-penetrating OCA-B peptide inhibitors normalized glucose levels, and reduced T cell infiltration and proinflammatory cytokine expression in newly-diabetic NOD mice. Together, the results indicate that OCA-B is a potent autoimmune regulator and a promising target for pharmacologic inhibition.

53 **Introduction**

54 Type 1 Diabetes (T1D) is an autoimmune disease in which the host immune system is directed towards
55 antigens associated with pancreatic beta cells[1, 2]. Pathologically, T1D is characterized by insulitis, beta
56 cell destruction and inability to produce insulin. The main treatment for T1D, life-long insulin therapy,
57 treats symptoms but not cause. The development of new T1D treatments is limited by an incomplete
58 understanding of disease mechanisms[3]. Beta cell regeneration is a promising line of therapy, but still
59 requires methods to specifically block T1D autoimmunity. An ideal method of therapy would be to
60 capture patients early in the disease course and block autoimmunity while keeping normal immune
61 function intact. Such a therapy would spare remaining beta cell function.

62 In $CD4^+$ T cells, the transcription factor Oct1 and its cofactor OCA-B regulate a set of ~150
63 target genes, including *Il2*, *Ifng* and *Csf2* (*Gmcsf*)[4]. Upon T cell activation, many of these targets are
64 activated by pathways that converge on transcription factors such as NF-AT, AP-1 and NF-κB. Factors
65 like NF-AT can be thought of as the primary on/off switches for these genes, and drugs that block NF-
66 AT activation effectively block their expression. Such drugs have utility in many contexts, but also
67 have drawbacks including global dampening of immune function and side effects due to expression in
68 other tissues. In contrast, Oct1 and OCA-B insulate silent but previously activated target genes against
69 stable repression. Loss of either protein does not affect $CD4^+$ T cell responses to stimulation in vitro or
70 primary infection in mice[4, 5], but causes large defects in target gene expression upon secondary
71 stimulation in vitro and defective $CD4^+$ memory T cell formation and recall responses in vivo[4, 6]. In
72 addition, OCA-B expression is largely confined to lymphocytes. OCA-B is silent in thymocytes and
73 naïve $CD4^+$ T cells, but is induced and stably expressed after sustained antigen stimulation[4]. Once
74 expressed, OCA-B recruits the histone lysine demethylase Jmjd1a/Jhdm2a/Kdm3a to Oct1 at target
75 loci, where it locally removes inhibitory H3K9me2 chromatin marks that would otherwise promote
76 repressive chromatin environments[4, 6]. OCA-B also potentiates polarization of activated helper T cells
77 towards the Th17 phenotype, among the most pro-inflammatory helper T cell subsets[7].

78 Persistent antigen exposure is a common property of autoimmune responses. Among profiled
79 $CD4^+$ T cell subsets, OCA-B levels are elevated in both central memory cells and pancreas-infiltrating,
80 islet-reactive cells (http://www.immgen.org/databrowser/index.html). Both Oct1 and OCA-B are
81 highly conserved to humans, and genome-wide association studies identify Oct1/OCA-B binding site
82 polymorphisms that confer predisposition to a variety of human autoimmune diseases including T1D,
83 multiple sclerosis, lupus, inflammatory bowel disease and rheumatoid arthritis[8, 9, 10, 11, 12, 13, 14]. Other

84 studies implicate polymorphisms at the *Ocab* (*Pou2af1*) locus itself in different forms autoimmunity[15,
85 16]. We therefore hypothesized that targeting OCA-B would inhibit diabetogenic T cell responses.
86 Here, we generate a T cell conditional mouse model of OCA-B deficiency. We show that
87 OCA-B ablation protects animals from spontaneous, polyclonal T1D. Protection was associated with
88 reduced T cell infiltration and proinflammatory cytokine expression. Conditional OCA-B deletion
89 maintained normal pancreatic lymph node cell populations, numbers, gene expression and TCR
90 clonality. In contrast, significant alterations in specific TCR clones were present in the pancreatic islets
91 of OCA-B T cell conditional mice. Protection from OCA-B loss varied among different TCR
92 transgenic and monoclonal antigen models, and was weakest using synthetic antigens and monoclonal
93 transplant models. Protection was stronger, but still incomplete, using a spontaneous CD8 TCR
94 transgenic model. Using a rational-design approach, we developed membrane-penetrating OCA-B
95 peptide inhibitors that are efficacious in vitro and in mice. Collectively, the results indicate that OCA-
96 B is a potent and pharmacologically accessible autoimmune regulator.

97 **Results**

98 **Generation of an *Ocab* conditional allele and NOD backcrossing.** We generated a conditional *Ocab*
99 (*Pou2af1*) mouse allele using embryonic stem cells provided by the knockout mouse project (KOMP)
100 repository. Deletion of the *LoxP* sites is predicted to create a null allele by disrupting the first three
101 exons (Fig. 1a). Breeding chimeric mice resulted in germline transmission and a founder mouse (Fig.
102 1B, lane 2) that was crossed to a FLP deleter mouse strain (FLP^{Rosa26}) to remove the reporter cassette
103 and create a floxed conditional allele (Fig. 1a and b, lane 3). Intercrossing these mice generated
104 homozygous *fl/fl* mice (Fig. 1b, lane 4). The mice were crossed to germline Cre deleter strain
105 (Cre^{Rosa26}) to generate null (*Δ*) alleles (lanes 5 and 6). As expected, homozygous *fl/fl* mice produce
106 normal amounts of both p34 and p35 OCA-B protein isoforms (Supplementary Fig. 1a, lane 6), while
107 no protein of either isoform is present in germline-deleted *Δ/Δ* spleens (lanes 7-8). These results
108 indicate that the *fl* allele is OCA-B sufficient and the Cre-deleted allele is a null. Crossing the *fl* allele
109 onto a Cre^{CD4} driver, which deletes in both CD4 and CD8 compartments, resulted in efficient deletion
110 in splenic T cells (Fig. 1b). These findings indicate that this allele represents a robust system in which
111 to study OCA-B function in T cells.

112 The *Ocab* (*Pou2af1*) conditional allele was generated on a C57BL/6 background. To test the
113 prediction that OCA-B expression in T cells promotes T1D emergence, we conducted speed congenic
114 backcrosses to the NOD strain background. This method allows spontaneous diabetes to be produced
115 rapidly by screening and selecting for 13 microsatellite and SNP markers associated with NOD
116 autoimmune susceptibility[17]. Backcrossing is facilitated by the fact that *Ocab* is located on mouse
117 chromosome 9 and is not nearby any of the *Idd* loci. Following these markers with specific primer
118 pairs (Supplementary Table 1), we produced backcrossed animals with all 13 markers (Supplementary
119 Fig. 1b) that recapitulate spontaneous autoimmunity (not shown). For example, *Idd1*, which maps to
120 the MHC region[18], converted to the homozygous NOD allele after 2 backcross generations
121 (Supplementary Fig. 1B, lane 3), whereas *Idd13*, which maps near beta-2-microglobulin[19] became
122 NOD homozygous after 4 generations (lane 4). Genotyping identified this fourth-generation
123 backcrossed animal as having all 13 microsatellite markers and the *Ocab* conditional allele
124 (Supplementary Fig. 1c, #122). This founder animal was crossed to NOD.Cre^{CD4} and the floxed allele
125 homozygosed in order to delete OCA-B in T cells to assess the effects on T1D. Similar NOD
126 backcrosses, conducted using *Ocab* null mice[20], resulted in OCA-B germline-deficient NOD mice
127 (data not shown). As with the original C57BL/6 OCA-B germline knockout[20], all alleles were viable
128 and fertile with no obvious health issues.

129

130 **Normal baseline T cell status in NOD mice lacking OCA-B.** To study broad effects of T cell-
131 specific OCA-B loss on T cell function, we performed single-cell RNA sequencing (scRNAseq) and
132 TCR clonotype analysis using $CD3^+$ T cells isolated from PLNs of pre-diabetic 8 week-old female
133 NOD.*Ocab*$^{fl/fl}$Cre^{CD4} or NOD.*Ocab*$^{fl/fl}$ littermate controls. For each group cells from three animals were
134 combined for microfluidics and subsequent sequencing. T cells were isolated from PLNs of three
135 animals in each group and combined for analysis. ~6000 knockout and ~3000 control cells were
136 identified in this analysis, most of which comprise naïve CD4 and CD8 cells (Supplementary Fig. 2a,
137 pink and orange), and regulatory T cells (Tregs, green). There was also a small population of activated
138 $CD4^+$+$CD8^+$ cells (green), presumably in the process of exiting the lymph nodes. Other than a small
139 decrease in the percentage of activated $CD4^+$+$CD8^+$ cells (4.4 vs 6.1%), few differences in the
140 populations were observed. None of these populations expressed measurable amounts of *Ocab*
141 (*Pou2af1*) mRNA (not shown), however *Pou2af1* is expressed at low levels in T cells making it
142 difficult capture by scRNAseq. In addition, few changes in gene expression were identified, and the
143 great majority of these were not of immunological interest (Supplementary Fig. 2b, Supplementary
144 Table 2). We also determined TCR repertoires in these T cell populations, identifying few changes as a
145 whole (Supplementary Fig. 2c). However, specific sub-populations did show changes in TCR
146 utilization. For example, NOD $CD8^+$ T cells expressing *Trbv13-3* (Vβ8.1) display reactivity to islet-
147 specific glucose-6-phosphatase catalytic subunit related protein (IGRP) and are associated with T1D[21].
148 Although this clone was unchanged across the entire population of T cells (Supplementary Fig. 2c), it
149 was over-represented in the effector $CD8^+$ population (Supplementary Fig. 2d). In contrast, other TCR
150 clonotypes such as *Trbv13-1*, *Trbv13-2*, *Trbv1* and *Trbv15* were unchanged (not shown). This result
151 was confirmed with flow cytometric staining of $CD8^+$ T cells using Vβ8.1 antibodies (Supplementary
152 Fig. 2e). This change was coupled with a decrease the presence of this particular clone in pancreatic
153 islets (below). These results indicate that OCA-B loss does not result in gross changes PLN T cell
154 repertoire or status, but results in lymph node retention of potentially autoreactive clones.
155

156 **NOD mice lacking OCA-B are protected from T1D.** T1D onset in NOD mice is spontaneous and
157 acute[22]. To test the impact of OCA-B loss in T cells on spontaneous T1D, we compared incidence in in
158 female NOD.*Ocab*$^{fl/fl}$Cre^{CD4} mice, and controls lacking the Cre^{CD4} driver. Glucose was monitored 2-3
159 times per week. Using a 250 mg/dL blood glucose cutoff, approximately 60% of *Ocab*$^{fl/fl}$ control mice
160 manifested spontaneous diabetes by 24 weeks of age, while no *Ocab*$^{fl/fl}$Cre^{CD4} mice became diabetic

161 (Fig. 1d). Blood glucose was stable in *Ocab*$^{fl/fl}$Cre^{CD4} females but began to spike in control mice
162 beginning at week 16, rising to an average of >300 mg/dL by 24 weeks (Fig. 1e). Similar results were
163 observed using female whole-body knockout NOD.*Ocab*$^{-/-}$ compared to *Ocab*$^{+/+}$ littermate controls.
164 While ~80% of control females developed T1D within 24 weeks after birth, only ~20% of
165 NOD.*Ocab*$^{\Delta/\Delta}$ females did so (Fig. 1f). Cumulatively, the results show that OCA-B expression in T
166 cells is critical for T1D pathogenesis in NOD mice.
167
168 **NOD.*Ocab* conditional mice have fewer islet macrophages and IFNγ–expressing cytotoxic T cells,**
169 **and more Tregs.** We sacrificed *Ocab*$^{fl/fl}$Cre^{CD4} female mice and controls at 8 and 24 weeks, and
170 determined the frequencies of immune cells in the pacreata. We observed more T cells in the pancreata
171 of OCA-B deficient mice (not shown). This result is understandable because the control mice have
172 annihilated their pool of beta cells, resulting in lack of antigen. We also studied pancreatic
173 macrophages in these mice. Islet infiltration of F4/80^{+}CD11b^{+} macrophages is critical for NOD T1D
174 pathogenesis both in spontaneous and adoptive transfer T1D models[23, 24]. CCL1 expressed in
175 diabetogenic CD4 T cells is known to recruit CCR8-expressing macrophages[25]. Interestingly, OCA-B
176 deletion in stimulated, rested and re-stimulated CD4^{+} T cells decreases *Ccl1* mRNA expression
177 compared to controls (Supplementary Table 3). We therefore hypothesized that OCA-B expression in
178 T cells is important for macrophage islet infiltration. Despite the fact that antigen and greater numbers
179 of T cells were present, we observed 5-fold fewer macrophages in 24 week-old NOD.*Ocab*$^{fl/fl}$Cre^{CD4}
180 islets (Fig. 2a,b). In contrast, macrophage numbers were unaffected by T cell-specific OCA-B loss in
181 pre-diabetic (8 week) mice (Fig. 2a).
182 IFNγ is a direct OCA-B target gene[4] and a strong promoter of T1D. Levels of serum and
183 pancreatic IFNγ gradually rise in young NOD mice, reaching maximum at diabetes onset[26].
184 Diabetogenic CD4^{+} and CD8^{+} T cells both express IFNγ in humans and NOD mice[27, 28, 29]. Therefore,
185 we predicted that OCA-B loss would reduce islet IFNγ expression in CD4^{+} and CD8^{+} T cells. We
186 compared IFNγ-expressing pancreatic CD4^{+} and CD8^{+} T cells in female NOD.*Ocab*$^{fl/fl}$Cre^{CD4} and
187 littermate control mice lacking Cre^{CD4}. In 12 week-old prediabetic mice, CD8^{+} T cell frequencies were
188 significantly decreased (Fig. 2c), whereas CD4^{+} T cells at the same timepoint were unchanged (data
189 not shown). At the time of diabetes onset (16 weeks), proportionally fewer IFNγ-expressing CD8^{+} T
190 cells were present in *Ocab* conditional-deleted mice compared to controls (Fig. 2d).
191 CD4^{+}CD25^{HI}FoxP3^{+} Tregs interfere with T1D development in NOD mice[30, 31]. Analysis of
192 previously generated RNAseq datasets shows that naïve *Ocab* null CD4^{+} T cells express 4-fold more

193 *Foxp3* mRNA compared to controls upon in vitro stimulation (Supplementary Table 3). To determine
194 whether the protection conferred by T cell conditional OCA-B is associated with changes in Tregs, we
195 analyzed pancreatic Treg frequencies, observing a trend towards more Tregs in pre-diabetic (8 week-
196 old) NOD.*Ocab*$^{fl/fl}$Cre^{CD4} mice compared to controls (Fig. 2e). Interestingly, there were no differences
197 late in disease course, at 16 or 24 weeks (data not shown).
198 If increased Treg numbers help mediate protection in NOD.*Ocab*$^{fl/fl}$Cre^{CD4} mice, then depletion
199 of these Tregs would be expected normalize T1D pathogenesis in knockout mice relative to controls.
200 Anti-CD25 antibody injection in neonatal NOD mice depletes Tregs (as well as activated T cells), and
201 accelerates T1D onset[32]. Surprisingly, we observed that anti-CD25 antibody-injected
202 NOD.*Ocab*$^{fl/fl}$Cre^{CD4} mice were still protected from T1D development relative to controls, though to a
203 lesser degree than in undepleted mice (Fig. 2f). These results support a conclusion that Tregs partly
204 contribute to the T1D protection in mice lacking OCA-B in their T cells.
205
206 **T cell-specific OCA-B deletion alters the islet-infiltrating TCR repertoire.** We performed
207 scRNAseq and TCR clonotype analysis similar to Supplementary Fig. 2, but using older (12 week) but
208 still pre-diabetic NOD.*Ocab*$^{fl/fl}$Cre^{CD4} or NOD.*Ocab*$^{fl/fl}$ littermate control female mice, and using total
209 CD45$^+$ cells isolated from pancreatic islets rather than PLNs. Cells were isolated from four animals per
210 group and combined for microfluidics and sequencing. After filtering, ~6200 knockout and ~3800
211 control cells were identified. Overlaying cell from both genotypes, we used their gene expression
212 profiles to definitively identify multiple cell lineages, including naïve CD4$^+$ + CD8$^+$ T cells,
213 memory/effector CD4$^+$ T cells, memory/effector CD8$^+$ T cells, B cells, macrophages and neutrophils
214 (Fig. 3a). The biggest relative change in populations was neutrophils, which decreased from 3.4 to
215 1.4% in conditional knockout islets (Fig. 3a). B cells were also decreased, albeit more slightly. These
216 changes were accompanied by an increase in the percentages of CD4$^+$ and CD8$^+$ T cells with naïve
217 phenotypes in conditional knockouts (31.7 vs. 25%). Like endpoint diabetic animals (Fig. 2a,b),
218 macrophage numbers were decreased but only slightly. Unlike PLNs, prediabetic islets showed
219 significant changes in gene expression between the two groups (Fig. 3b), the strongest of which
220 occurred in neutrophils (e.g., *Cxcl2*, down), memory/effector CD8$^+$ T cells (*Ccl4*, *Tcrg-v1*, *Itga*, down;
221 *Tcrbv1*, *Trav8n-2*, up), NK T cells (*Klra2*, *Lars2*, down) and γδT cells (*Gzma*, *Gzmb*, *Ccl5*, down).
222 We also profiled TCR clonality in pancreatic T cells. Across total T cells, few changes were
223 observed (Supplementary Fig. 3), however this was largely to do similar representation in the naïve T
224 cell pool. Isolating just antigen-experienced CD4$^+$ and CD8$^+$ effector + memory subpopulations

225 revealed sharp differences. For example, polyclonal NOD mice $CD8^+$ T cells expressing *Trbv13-3*
226 (Vβ8.1) display reactivity to IGRP and are associated with T1D[21]. Relative to controls, this clonotype
227 was under-represented in OCA-B deficient effector + memory $CD8^+$ cells (Fig. 3c, 20.9% vs 8.6%).
228 Approximately half of these cells showed reactivity to $IGRP_{206-214}$ based on tetramer staining (data not
229 shown). Based on this information, we repeated the clonotype analysis, but only using the effector +
230 memory $CD8^+$ T cell cluster. Within this population, dominant TCR clonotypes used by conditional
231 and control T cells were strikingly different (Fig. 3d). Clonotype 1 for example corresponds to a TCRα
232 V8N-2 chain paired with TCRβ V1 or V15 and has not been associated with T1D. This clonotype was
233 absent in control islets but represented >4% of OCA-B deficient islet $CD8^+$ effector + memory T cells
234 (Fig. 3d). Clonotype 1 cells overlaid with both genotypes is shown in Fig. 3e. Clonotype 2 by contrast
235 is associated with the T1D-associated Vβ13.3 β chain. This clonotype was strongly represented in
236 controls (>3%) but absent from experimental effector + memory $CD8^+$ cells (Fig. 3d). In contrast to
237 CD8-dominant TCR clonotypes, CD4-dominant TCRs associated with T1D were still present in
238 knockouts, but associated with markers of anergy. For example, clonotype 4 (*Trav13-1/16N+Trbv15*)
239 is associated with pro-diabetogenic, BDC-reactive $CD4^+$ T cells[33]. This clonotype was enriched in the
240 OCA-B deficient effector + memory $CD4^+$ cells, but only in a CTLA4- and FR4-expressing sub-
241 population (Fig. 3e). Cumulatively, these results indicate that OCA-B loss from T cells significantly
242 skews the landscape of islet effector/memory-like T cells, in particular $CD8^+$ T cells, to an anti-
243 diabetogenic phenotype.
244
245 **Protection conferred by OCA-B loss is model-specific.** T1D in NOD mice originates from defective
246 negative selection in developing T cells, resulting in T cell autoreactivity. OCA-B is not expressed in
247 thymocytes and OCA-B loss does not appear to affect T cell development[4]. Therefore, the protective
248 effect of OCA-B loss in T cells likely arises from blunting pre-existing autoreactivity in the periphery.
249 To test the hypothesis that OCA-B loss confers protection in simplified systems, we crossed OCA-B
250 deficient mouse models employing TCR transgenes and model antigens.
251 Depleting Tregs and transferring remaining T cells from BDC2.5 TCR transgenic mice into
252 NOD.Scid mice results in disease after approximately 10 d[34, 35]. We crossed the germline null *Ocab*
253 allele to BDC2.5 mice to test the effect of OCA-B in this model. We transferred $CD4^+CD25^-$ T cells
254 from germline $Ocab^{-/-}$ or $Ocab^{+/+}$ BDC2.5 mice into NOD.Scid recipients, monitoring diabetes
255 emergence. Transplants from both $Ocab^{-/-}$ and control NOD.BDC2.5 mice resulted in equivalent
256 disease kinetics (Fig. 4a) and severity (not shown). Transferring $CD4^+CD62L^+V\beta^+$ T cells from $Ocab^{-/-}$

257 and control NOD.BDC2.5 mice into NOD.Scid recipients also showed no difference between the
258 experimental and control groups (Supplementary Fig. 4a). Negative results were also generated by
259 transplanting total $CD4^+$ T cells into immunodeficient NCG recipients (Fig. 4b). We also tested the
260 effect of T cell conditional OCA-B deletion in a different strain background, C57BL/6J, using the
261 artificial membranous ovalbumin antigen expressed from the rat insulin promoter (RIP-mOVA)[36]. In
262 this experiment, wild-type OVA-reactive $CD8^+$ OT-I T cells were transferred into either *Ocab*$^{fl/fl}$Cre^{CD4}
263 or control *Ocab*$^{fl/fl}$ RIP-mOVA mice. Host $CD4^+$ T cells help transferred OT-I T cells promote T1D
264 pathogenesis in this model[37]. Mice were then infected with Lm-OVA to induce strong and synchronous
265 beta cell destruction and loss of glucose control (>400 mg/dL). No differences were observed
266 (Supplementary Fig. 4b). These results indicate that OCA-B does not act analogously to transcription
267 factors that act as a primary on/off switches, such as NF-AT. Knockouts of these factors would result
268 in broad immunosuppression and protection from T1D in all models. Rather, our results suggest that
269 the effects of OCA-B loss may protect from autoimmunity in specific contexts, including polyclonal
270 contexts. To test this supposition, we also performed transplant experiments using total splenocytes
271 from polyclonal NOD.*Ocab*$^{fl/fl}$Cre^{CD4} mice or controls. Using this transplant system, robust T1D
272 protection with T cell-specific OCA-B loss was observed (Fig. 4c). This protection was associated with
273 fewer IFNγ-expressing cytotoxic T cells in the islets of OCA-B T cell conditional NOD mice (Fig. 4d),
274 and less insulitis in histological sections of pancreata (Fig. 4e,f).
275 NY8.3 transgenic mice express a CD8-restricted TCR directed towards $IGRP_{206-214}$ and
276 manifest spontaneous T1D[38]. The NY8.3 clonotype was significantly attenuated in the islets of T cell
277 conditional OCA-B deficient mice (Fig. 3c,d,e). We also crossed the *Ocab* germline allele NY8.3,
278 passively monitoring *Ocab*$^{-/-}$ or littermate control *Ocab*$^{+/+}$ NY8.3 mice for T1D development.
279 Significant protection was observed (HR=0.4472, p=0.0352), though the degree of protection was less
280 than in polyclonal models (Fig. 4g). Together with the observed depletion of autoreactive CD8 clones
281 from OCA-B deficient pancreatic islets, this result indicates that OCA-B promotes T1D in peripheral
282 auto-reactive T cells in part directly through the $CD8^+$ cells. Using immunoblotting with OCA-B
283 antibodies, we confirmed OCA-B expression in primary splenic C57BL/6 $CD8^+$ T cells. OCA-B is
284 undetectable in naïve splenic $CD4^+$ cells but becomes induced with prolonged activation[4]. Unlike
285 $CD4^+$ cells (Fig .4h, top panels), OCA-B^+ could be detected in naïve cells (Fig. 4h, lane 1). Expression
286 was augmented more rapidly in $CD8^+$ cells upon T cell activation using CD3ε/CD28 antibodies (lane
287 2). Similar to $CD4^+$ cells, expression was stably maintained when the stimulus was removed and cells
288 were rested with IL-2 (lane 6).

289

290 **OCA-B deficiency promotes CD4$^+$ T cell anergy in vitro.** Our scRNAseq data indicate that CD8-
291 restricted TCR clones associated with T1D are depleted from the islets of OCA-B T cell conditional
292 mice. In contrast, CD4-restricted clones were increased but associated with an anergic phenotype (Fig.
293 3e). Anergy is a peripheral tolerance mechanism in which T cells that encounter TCR signals without
294 co-stimulation become nonfunctional to protect from autoreactivity[39, 40, 41]. Normal naïve primary
295 CD4$^+$ T cells can be activated in culture by TCR and costimulatory receptor activation, e.g. with anti-
296 CD3ε/CD28 antibodies. Providing TCR signals (via immobilized anti-CD3ε monoclonal antibodies) to
297 naïve T cells in culture generates anergic responses[42]. Loss of Oct1, the transcription factor with which
298 OCA-B docks, augments anergic responses in this assay[5]. Interestingly, OCA-B protein is induced to
299 the same extent in naïve CD4$^+$ T cells stimulated with only anti-CD3ε antibodies as with co-
300 stimulation (Fig.5a). To determine if OCA-B loss promotes anergic CD4$^+$ T cell responses, we
301 stimulated naïve splenic CD4$^+$ T cells from germline knockout *Ocab*$^{-/-}$ and control *Ocab1*$^{+/+}$ animals
302 ex vivo using plate-bound anti-CD3ε antibodies without co-stimulation, and restimulated the cells with
303 PMA/ionomycin. Following restimulation, CD4$^+$ T cells lacking OCA-B generated 2.5-fold less IL-2
304 (Fig. 5b,c), indicating that OCA-B provides a barrier against anergic responses.
305 ICOS (Inducible T-cell Costimulator) has an important role in the induction of T cell anergy
306 and is down-regulated by Oct1 loss in T cells[43, 44, 45]. Similarly in CD4$^+$ cells, elevated expression of
307 FR4 and CD73 is associated with anergy and higher in Oct1-deficient compared to control cells[39, 46].
308 To determine whether OCA-B affects in the protein related to T cell anergy, we harvested pre-
309 activated CD4$^+$CD44$^+$ T cells from the spleens of *Ocab*$^{fl/fl}$Cre^{CD4} and littermate control Cre^{CD4} animals,
310 and re-stimulated them for 24 hr ex vivo using anti-CD3ε antibodies ± co-stimulation using anti-CD28
311 antibodies. CD4$^+$CD44$^+$FR4^{hi}CD73^{hi} anergic cells were ~2 fold more strongly induced in T cells
312 lacking OCA-B (Fig. 5d). ICOS levels were similarly elevated in the OCA-B deficient condition (Fig.
313 5e). Additionally, and consistent with prior data[5], the expression of the activation marker CD25 was
314 decreased (Fig. 5f). These results suggest that OCA-B loss creates a requirement for CD28 co-
315 stimulation in secondary stimulation situations, effectively instituting higher immune checkpoint
316 thresholds in order for cells to become fully re-activated.
317

318 **Generation of an OCA-B peptide inhibitor.** The normal T cell developmental and primary immune
319 response phenotypes observed with OCA-B genetic deletion suggested the possibility of a "therapeutic
320 window" in which targeting OCA-B pharmacologically would leave baseline immune function only

321 minimally affected. Drugs that target transcription factors and protein-protein interactions are now
322 entering clinical use[47, 48]. Pre-clinical membrane-penetrating peptides have also been developed that
323 successfully target transcription factors such as BCL6[49]. Based on the co-crystal structure of the Oct1
324 DNA-binding domain, the OCA-B N-terminus and consensus binding DNA[50], we applied rational-
325 design principles to generate a membrane-permeable peptide inhibitor of OCA-B's downstream
326 effector functions in order to target OCA-B pharmacologically.

327 In $CD4^+$ T cells, Oct1 interacts with Jmjd1a in a MEK/ERK-dependent manner[4, 6]. Oct1
328 contains two consensus ERK phospho-acceptor serines. The structure of the Oct1 DNA binding
329 domain complexed with consensus octamer binding site DNA[51] reveals that these Oct1 serines are
330 located in a flexible, solvent-exposed loop (the linker domain), which connects the two DNA binding
331 sub-domains (Fig. 6a, red dashed line). In contrast with Oct1, OCA-B constitutively interacts with
332 Jmjd1a[4]. The OCA-B N-terminus has been solved in complex with Oct1 and consensus octamer
333 DNA[50]. The crystalized region of OCA-B is known to include regions critical for both Oct1 binding
334 and transcription activity[52]. To identify potential Jmjd1a-interacting OCA-B regions, we aligned the
335 full-length Oct1 and OCA-B amino acid sequences to a region of androgen receptor (AR) known to
336 interact with Jmjd1a[53]. Human AR mutations that cause androgen insensitivity have been mapped to a
337 cofactor interaction surface spanning residues 698-721[54]. Aligning this sequence to full-length Oct1
338 identified the linker domain as the top hit (Fig. 6b), implicating the Oct1 linker as a potential Jmjd1a-
339 interacting surface. The alignment shows conservation of 3 out of 4 sites of deleterious AR mutation
340 (asterisks) with Oct1. The mutation site that is not conserved is a consensus ERK target in Oct1, and a
341 phospho-mimetic glutamic acid residue in AR (blue box). These findings suggest that the Oct1 linker
342 domain constitutes a surface which, when phosphorylated by ERK, interacts with Jmjd1a.

343 As with Oct1, alignment with OCA-B identifies a potential Jmjd1a interacting surface (Fig.
344 6b). Unlike Oct1, an OCA-B glutamic acid residue (Glu30) aligns with AR, consistent with the finding
345 that OCA-B constitutively interacts with Jmjd1a in the absence of ERK signaling[4]. Furthermore, the
346 OCA-B residues aligning to AR lie on one side of a short, solvent-exposed alpha-helix (Fig. 6a). Glu30
347 (red), Leu31 (yellow), Arg34 (blue) and His38 (blue) may therefore constitute a Jmjd1a docking
348 surface. These residues are conserved to humans (Fig. 6c). We mutated OCA-B L31 and R34 to
349 alanines in a transient expression plasmid to test the effect on the Jmjd1a interaction, and transfected
350 the double-point mutant or parent plasmid control into HCT116 cells, which do not express
351 endogenous OCA-B. Control co-IP using Jmjd1a antibodies and wild-type OCA-B confirms the
352 published interaction (Fig. 6d, lane 5), while the mutant OCA-B protein failed to interact (lane 8). The

353 mutant was expressed equivalently to WT in HCT116 cells (lanes 2, 3). These results show the
354 importance of OCA-B residues 30-38 for the interaction with Jmjd1a.
355 To identify potential OCA-B competitive inhibitors, we synthesized three overlapping peptides
356 corresponding to the OCA-B N-terminus (Fig. 6e, peptides #1, #2 (hereafter called "JumOCA") and
357 #3), as C-terminal fusions to the HIV Tat protein for membrane permeability[55]. Initial preparations
358 were conjugated to FITC to track the peptide. Incubating peptides with total splenic or pancreatic
359 $CD3^+$ T cells in culture with 45 μM Tat-fused peptide for 15 min resulted in significant concentration.
360 Control OVA-fused peptide showed no such effect (Supplementary Fig. 5). We then treated splenic
361 $CD4^+$ T cells with the Tat-fused peptides (lacking FITC) in ex vivo culture. Prior work has shown that
362 6 hr restimulation of resting but previously activated cells reveals sensitivity to OCA-B loss[4]. Using
363 this assay with 50 μM JumOCA peptide (every other day with media changes during rest and
364 restimulation) inhibited *Il2* mRNA expression relative to β-actin by ~10-fold (Fig. 6f, compare Tat
365 peptide to JumOCA). Although treated cells showed no obvious changes in viability, morphology or
366 expansion during the course of the assay (not shown), there was a 2-3-fold nonspecific diminution of
367 activity associated with unfused Tat peptide (Fig. 6f, compare Tat peptide with no peptide). The Tat
368 membrane-penetrating peptide has been associated with toxicities[49, 56, 57]. Similar results were obtained
369 with the larger peptide #3 but not with peptide #1 (not shown). Peptide #1 is missing residues
370 important for the Jmjd1a interaction based on mutagenesis (Fig. 6b). For all further experiments, we
371 exclusively used the JumOCA peptide.
372 We then synthesized a Tat-conjugated peptide using a scrambled JumOCA sequence. This
373 peptide has the same amino acid composition, mass and pI, but lacks the OCA-B primary amino acid
374 sequence and should not be able to efficiently compete for Jmjd1a. We used the Tat-only, scrambled
375 and JumOCA peptides in assays similar to Fig. 6f, except using flow cytometry to assay endpoint IL-2
376 production. JumOCA significantly inhibited IL-2 production relative to the scrambled control,
377 however there were significant toxicities associated with both the scrambled and Tat-only peptides
378 relative to vehicle (Fig. 6g). An example mouse from this experiment is shown in Fig. 6h.
379 The above results are consistent with the JumOCA peptide operating through a Jmjd1a
380 competitive inhibition mechanism. To test this directly, we used scrambled, double point mutant and
381 wild-type (JumOCA) peptides lacking Tat in a Jmjd1a co-IP assay. We subjected lysates from mouse
382 M12 B cells, which expresses endogenous OCA-B, to immunoprecipitation with Jmjd1a antibodies,
383 resulting in efficient OCA-B co-IP (Fig. 6i, lane 3). Incubation of precipitated material with scrambled

384 or double point mutant peptides had no effect on OCA-B co-immunoprecipitation (lanes 4-5), while
385 the same concentration of JumOCA peptide efficiently blocked OCA-B recovery (lane 6).
386
387 **An OCA-B peptide inhibitor protects NOD mice from newly-arisen diabetes.** By the time
388 symptoms arise in NOD mice, 90-95% of beta cells have been destroyed. Remaining beta cells are
389 rendered nonfunctional due to insulitis. Alleviating this inflammation provides a "honeymoon period"
390 during which glucose homeostasis can be restored. We treated 14-18 week-old littermate female NOD
391 mice whose glucose levels were newly-risen above 225 mg/dL but still below 275 mg/dL with three
392 intravenous injections of 10 mg/kg peptide or Tat-only peptide control. Injections were spaced 12 hr
393 apart. 12 hr after the final injection, blood glucose was collected and flow cytometry performed on the
394 pancreas and PLNs. Strikingly, the inhibitor reversed elevated blood glucose (Fig. 7a). Control peptide
395 at the same concentration had no effect. Islet T cell infiltration and pro-inflammatory IFNγ and IL-17A
396 cytokine production were strongly reduced by JumOCA peptide treatment compared to controls (Fig.
397 7b,c). In contrast to the pancreas, PLNs showed no change in T cell numbers or percentages (Fig. 7d)
398 but similar changes in pro-inflammatory cytokine production (not shown). These data provide
399 evidence that targeting OCA-B is a valid strategy to treat emerging T1D, potentially with minimal side
400 effects, and identify a first-generation inhibitor that is efficacious in vivo.

401 **Discussion**

402 Here we show that targeting OCA-B genetically or pharmacologically can block T1D in mouse
403 models. OCA-B is a transcriptional coregulatory protein named for its strong expression in the B cell
404 lineage, where it is dispensable until after B cell activation, where it is essential for the generation of
405 germinal centers[58]. OCA-B is not expressed during thymic development or in naïve CD4 T^+ cells, but
406 is stably induced upon T^+ cell activation. In contrast, OCA-B is expressed in $CD8^+$ T cells, albeit at
407 lower levels compared to activated T cells. In both populations, OCA-B expression is maintained after
408 T cell stimulation has ceased.

409 In $CD4^+$ T cells, OCA-B associates with the POU-domain transcription factor Oct1 at ~150
410 immunomodulatory genes – among them *Il2*, *Ifng*, *Il17a* and *Csf2* (*Gmcsf*). Unlike transcription factors
411 such as NF-AT, AP-1 and NF-kB that act as primary "on" switches via direct gene activation, OCA-B
412 removes inhibitory chromatin modifications to establish permissive chromatin environments that allow
413 for silent but previously activated targets to be robustly expressed later[4, 6]. More specifically, OCA-B
414 interacts with Jmjd1a/Kdm3a, a histone lysine demethylase that removes inhibitory histone H3 lysine 9
415 methyl marks. OCA-B target gene expression is unchanged upon primary stimulation of cultured Oct1-
416 or OCA-B-deficient T cells, but upon secondary stimulation (a model of antigen reencounter) the
417 normally observed increased expression does not occur[4, 6]. In vivo, OCA-B loss leaves T cell
418 development and pathogen response unaffected, but impairs the establishment of new central memory
419 $CD4^+$ T cells. The few cells that are formed respond poorly to antigen re-encounter[4]. Repeated antigen
420 encounters that drive high levels of proinflammatory cytokines are a key feature of autoimmunity. In
421 both mice and humans, memory or memory-like cells can underlie autoimmunity including T1D[59, 60,
422 61].

423 The NOD model of T1D is spontaneous but only partially penetrant, much like the human
424 disease[62]. 60-80% of female NOD mice develop T1D in standard environments[22]. We find that
425 prediabetic OCA-B T cell deficient NOD mice harbor normal T cell numbers and similar TCR
426 specificities in their PLNs, consistent with prior observations that OCA-B deficient T cells are
427 immunocompetent[4]. Nevertheless, T cell conditional OCA-B knockouts are fully protected from
428 spontaneous T1D. Protection is associated with reduced islet leukocyte infiltration and reduced
429 proinflammatory cytokine expression. Whole-body NOD *Ocab* knockouts are also protected from
430 T1D, though to a lesser degree. Prior work showed that OCA-B whole-body knockout protects mice in
431 a MOG/EAE model of multiple sclerosis[63]. In contrast, a second study showed that OCA-B whole
432 body knockout exacerbates systemic, antibody-driven autoimmunity in *Sanroque* mice[64]. The
433 protective vs. exacerbating effects in these models may be due to effects on BCR repertoire[65]. T cell-

434 specific knockout of Oct1, a transcription factor with which OCA-B docks, blocks EAE but leaves
435 responses to infection with neurotropic viruses intact[5]. Together these data indicate that in T cells Oct1
436 and OCA-B promote autoimmunity including T1D, but that their role in B cells may be more complex.
437 OCA-B is typically expressed ~50-fold higher in B cells compared to T cells. A correctly calibrated
438 dose of competitive inhibitor could therefore be used to selectively blunt T cell-mediated
439 autoimmunity.

440 scRNAseq experiments reveal decreased neutrophil infiltration and an increase in the
441 percentage of T cells with a naïve phenotype in prediabetic OCA-B conditional knockout islets. Gene
442 expression changes were also identified that were consistent with antidiabetogenic effects of OCA-B T
443 cell knockout. For example, the remaining islet neutrophils in knockout mice show strong reductions in
444 *Cxcl2* expression compared to littermate controls. Cxcl2 is a potent neutrophil chemoattractant that
445 promotes T1D in vivo[66, 67], and therefore reductions in Cxcl2 may contribute to the reduced neutrophil
446 representation. Strikingly, OCA-B T cell deficient mice also lacked T1D-associated TCR clones in
447 their activated/memory CD8 pool. CD4 clonotypes associated with T1D were present, but associated
448 with anergy. Consistently, OCA-B loss promotes $CD4^+$ T cell anergy in vitro.

449 BDC2.5 and NY8.3 TCR transgenic mice are simplified monoclonal systems that allow easy
450 tracking of uniform T cell responses to antigens in vivo[68]. To test if OCA-B loss confers protection in
451 simplified monoclonal systems, we crossed the germline OCA-B null allele to these models, as well as
452 to RIP-mOVA transgenic mice on the C57BL/6 background. The latter mice express synthetic
453 membranous chicken ovalbumin in their thymi and pancreatic beta cells[69]. We crossed whole-body
454 null mice to the BDC2.5 transgenic line[70], which expresses a CD4-restricted TCR specific for a hybrid
455 insulin-chromogranin A peptide[71]. BDC2.5 autoreactive cells migrate to the islets and cause insulitis
456 beginning at 3-4 weeks. Due in part to Tregs that have escaped allelic exclusion, in many animals
457 insulitis is limited and does not progress to full-blown T1D. However, transferring $CD4^+CD62L^+V\beta^+$
458 or $CD4^+CD25^-$ T cells from BDC2.5 donor mice into NOD.SCID recipients results in rapid (7-10 d)
459 disease onset[34]. Transplants from both control and OCA-B null NOD/BDC2.5 mice resulted in disease
460 with similar kinetics. Identical results were also generated by depleting $CD25^+$ Tregs, or by
461 transplanting total $CD4^+$ T cells into immunodeficient NCG recipient mice. OCA-B loss also had no
462 effect using the RIP-mOVA model on the C57BL/6 background. This model expresses a synthetic
463 antigen, membranous chicken ovalbumin, in thymic epithelial and pancreatic beta cells[36].

464 In contrast to BDC2.5 and RIP-mOVA, NY8.3 transgenic mice carry a monoclonal CD8-
465 restricted TCR directed towards $IGRP_{206-214}$ and manifest spontaneous T1D[38]. Unlike BDC2.5

466 transplant models, OCA-B T cell conditional NY8.3 mice showed significant protection, though unlike
467 polyclonal NOD mice protection was incomplete. Cumulatively, the results are consistent with a model
468 in which OCA-B loss does not simply block T cell functionality, but rather desensitizes autoreactive T
469 cells. Because transgenic TCR models have fixed affinities to antigens that can be present throughout
470 disease or arise at specific points during disease etiology, they result in graded levels of disease. By
471 shifting the autoreactivity of different T cells along a spectrum of disease potentials, OCA-B loss can
472 result in full or partial protection in models with low and intermediate disease thresholds, whereas
473 models with high disease potentials remain autoreactive. Although protection in some of the more
474 severe models is likely to be inseparable from immunodeficiency, our results show that genetic
475 ablation of OCA-B strongly protects NOD animals from spontaneous T1D, and results in graded
476 protection that drops off with severity of the model. These properties make OCA-B a promising target
477 for pharmaceutical inhibition.

478 Recent work indicates that the prevailing idea that transcription regulators and protein-protein
479 interactions are "undruggable" is erroneous[47, 48, 72]. Pre-clinical membrane-penetrating peptides have
480 also been developed that successfully target transcription factors such as BCL6[49]. We applied rational-
481 design principles to generate a membrane-permeable competitive peptide inhibitor of the interaction
482 between OCA-B and a downstream effector, Jmjd1a/Kdm3a. This inhibitor corresponds to a region of
483 the OCA-B N-terminus, which is known to include residues critical for Oct1 binding and transcription
484 activity[52]. We tested the effect of this inhibitor, termed JumOCA, on T1D onset and severity. The
485 JumOCA sequence does not coincide with other sequences in the human or mouse proteome and is not
486 predicted to be strongly immunogenic. Peptide administration into NOD mice protected animals from
487 newly-arisen T1D and significantly reduced islet-infiltrating T cell numbers and cytokine production,
488 while having more mild effects on the PLNs. OCA-B levels in B cells are at least 50-fold higher than
489 in T cells (immgen.org)[73], making it likely that the observed effects are due to inhibition in T cells. The
490 preservation of normal PLN functionality both with peptide treatment and OCA-B genetic ablation
491 suggests a potential therapeutic window in which targeting OCA-B may leave baseline immune
492 function unaffected. While these peptides are unlikely to be used in a clinical setting, they offer proof-
493 of-principle for OCA-B as a therapeutic target, and can be used as tools for the further development of
494 therapeutics.

495 **Methods**

496 **Laboratory mice.** NOD/ShiLtJ, NOD.Scid (NOD.Emv302/2.CB17-Prkdcscid), BDC-2.5 TCR
497 transgenic, NY8.3 TCR transgenic and all breeder mice were maintained in a specific pathogen-free
498 research colony. NCG (NOD-Prkdc^{em26Cd52}Il2rg^{em26Cd22}/NjuCrl) mice were purchased from Charles
499 River Laboratories. NOD.Cre^{CD4} breeding pairs were a gift from Alexander Chervonsky (University of
500 Chicago). All animal experiments were approved by the University of Utah Institutional Animal Care
501 and Use Committee (IACUC approval 17-05008).

502

503 **Generation of *Ocab* (*Pou2af1*) conditional mice.** *Pou2af1*$^{tm1a(KOMP)Wtsi}$ mice were provided by the
504 knockout mouse project (KOMP) repository (University of California, Davis). Mice were derived from
505 embryonic stem cell clone EPD0761_3_B03, generated by the Wellcome Trust Sanger Institute. These
506 cells were derived from C57BL/6N mice, but subsequent mouse crosses were to C57BL/6J (>20
507 generations) for the RIP-mOVA model and NOD (four congenic backcrosses plus an additional
508 backcross to NOD.Cre^{CD4}). The embryonic stem cells contain a CSD-targeted allele[74]. The presence of
509 WT (582 bp) and Post-FLP (700 bp) alleles was determined by PCR using CSD-Pou2af1-F and CSD-
510 Pou2af1-ttR primers. The presence of the null (801 bp) allele was determined using CSD-Pou2af1-F
511 and CSD-Pou2af1-R primers. The presence of the floxed (359 bp) allele was determined using CSD-
512 Lox-F and CSD-Pou2af1-R primers. Primer sequences were as follows: CSD-Pou2af1-F,
513 5'TACAGAGAGACTAGACACGGTCTGC; CSD-Pou2af1-R,
514 5'GATGAGGACTCTGGGTTCAGAGAGG; CSD-loxF, 5'GAGATGGCGCAACGCAATTAATG;
515 CSD-Pou2af1-ttR, 5'AGAAGGCCTCGTTACACTCCTATGC. *Ocab* conditional mice were bred with
516 mice expressing Cre under the control of the CD4 promoter.

517

518 **Backcrossing *Ocab* germline null and conditional mice to the NOD background.** To generate
519 *Ocab*$^{-/-}$ and *Ocab* conditional mice on the NOD background, the previously described C57BL/6 *Ocab*
520 germline null allele[20] and the newly-generated *Ocab* conditional allele were backcrossed to NOD
521 ShiLt/J mice using congenic markers based on Mouse Genome Informatics
522 (http://www.informatics.jax.org) (Supplementary Table 1).

523

524 **Diabetes development and assessment.** Diabetes was monitored using blood glucose test strips
525 (Contour, Bayer). Mice with blood glucose levels >250 mg/dL were considered diabetic.

526

527 **Leukocyte isolation and intracellular cytokine staining.** Pancreatic lymph nodes were grinded and
528 passed through a nylon strainer. Pancreatic leukocytes were isolated as described previously[75]. Briefly,
529 pancreata were chopped and digested using collagenase IV (1 mg/mL, Gibco) in DMEM containing
530 1% fetal bovine serum (FBS, Rocky Mountain Biologicals) and 10 units of DNase I for 15 min at
531 37°C. The digested tissues were passed through a 70 μm strainer. Red blood cells were lysed by ACK
532 (Ammonium-Chloride-Potassium) lysis buffer (150 mM NH_4Cl, 10 mM $KHCO_3$, 0.1 mM Na_2EDTA).
533 For intracellular cytokine staining, cell suspensions in RPMI medium supplemented with 10% FBS
534 were re-stimulated for 4 hr with phorbol 12-myristate 13-acetate (PMA, Sigma, 50 ng/mL) and
535 ionomycin (Sigma, 1 μg/mL) in the presence of Brefeldin-A (GolgiPlug, BD Bioscience, 1 μl/ml), and
536 fixed by cell fixation/permeabilization solution (BD Cytofix/Cytoperm) according to the
537 manufacturer's protocol. Antibodies used for flow cytometry were as follows: FITC-conjugated anti-
538 mouse CD4, PE-conjugated anti-mouse CD45, PE-conjugated anti-mouse FR4 (Biolegend), PerCP-
539 conjugated anti-mouse CD8a, APC-conjugated anti-mouse IFNγ, PE-conjugated anti-mouse IL-17,
540 PerCP-conjugated anti-mouse CD11b, APC-conjugated anti-mouse F4/80, PE-conjugated anti-mouse
541 Gr-1, PE-conjugated anti-mouse ICOS (eBioscience), PerCP-conjugated anti-mouse FoxP3, V450-
542 conjugated anti-mouse CD73 (BD Bioscience) FITC-conjugated anti-mouse Vβ8.1/8.2 (Invitrogen).
543
544 **T cell adoptive transfer.** 6–8 wk old NOD.Scid recipient mice were injected retro-orbitally with
545 2×10^5 of splenic $CD4^+CD25^-$ T cells from pre-diabetic *Ocab*$^{-/-}$ or *Ocab*$^{+/+}$ NOD.BDC2.5 donors (6–8
546 wk old, sex-matched). T cells were purified using a $CD4^+CD25^+$ T cell isolation kit (Miltenyi). For
547 $CD4^+CD25^+Foxp3^+$ T cells, 1.5×10^6 purified splenic $CD4^+$ T cells from pre-diabetic, BDC2.5
548 transgenic NOD.*Ocab*$^{-/-}$ or NOD.*Ocab*$^{+/+}$ mice were transferred to sex-matched 6-8 wk old NCG
549 recipients (University of Utah pre-Clinical Resource Core) as previously described[35]. For total splenic
550 transfer experiments, 5×10^6 splenocytes from pre-diabetic NOD.*Ocab*$^{fl/fl}$ or NOD.*Ocab*$^{fl/fl}$Cre^{CD4} mice
551 were transferred into sex-matched 6-8 week-old NOD.Scid recipients mice as described previously[35].
552
553 **In vivo Treg depletion.** Anti-CD25 antibody in PBS (1 mg/mouse, Clone PC61, BioXCell) was
554 administered intraperitoneally to NOD.*Ocab*$^{fl/fl}$ or NOD.*Ocab*$^{fl/fl}$Cre^{CD4} mice twice (10 and 17 d after
555 birth) as previously described[32].
556
557 **In vitro culture of CD4 T cells.** For anergic cell induction, spleens were harvested from
558 NOD.*Ocab*$^{fl/fl}$Cre^{CD4} or control NOD.*Ocab*$^{fl/fl}$ animals. Single-cell suspensions were generated by

559 grinding and passage through 70 µm strainers. $CD4^+$ T cells were isolated using a mouse $CD4^+$ T cell
560 isolation kit (Miltenyi Biotec). Isolated $CD4^+$ T cells were cultured and stimulated with 5 µg/ml plate-
561 bound anti-CD3ε (BD Bioscience) and/or 2 µg/ml anti-CD28 antibodies (eBioscience) as described
562 previously[5]. For OCA-B inhibitor peptide treatments, naïve CD4 T cells were isolated from WT
563 C57BL/6 mice using a mouse naïve $CD4^+$ T cell isolation kit (Miltenyi Biotec) and cultured as
564 described previously[6]. For the in vitro experiments with OCA-B inhibitor peptides, indicated
565 concentrations of OCA-B inhibitor or control peptides were incubated with cells, with media changes
566 every 2 days after primary stimulation. Activation of C57BL/6 $CD4^+$ cells and subsequent profiling of
567 anergic responses was performed identically to[5].
568
569 **Single cell RNA sequencing.** $CD3^+$ T cells were isolated from 8 week-old NOD.*Ocab*$^{fl/fl}$ or
570 NOD.*Ocab*$^{fl/fl}$Cre^{CD4} females using a pan T cell isolation kit (Miltenyi). $CD45^+$ pancreatic leukocytes
571 were isolated from 12 week-old NOD.*Ocab*$^{fl/fl}$ or NOD.*Ocab*$^{fl/fl}$Cre^{CD4} females were isolated by flow
572 cytometry using a FACS Aria instrument (Becton-Dickinson). For each condition, cells were isolated
573 from three mice and combined. Cells were processed using the 10× Genomics Chromium platform
574 according the manufacturer's instructions. Paired-end high-throughput sequencing (125 cycles) was
575 performed via an Illumina NovaSeq instrument. Sequencing reads were processed by using 10×
576 Genomics CellRanger pipeline and further analyzed using the Seurat R package. Analysis of cells used
577 a standard filtering protocol removing cells with unique feature counts of >4,000 or <500, as well as
578 cells that have >5% mitochondrial counts (indicative of dead cells). No more than 15% of total cells
579 were removed by this process.
580
581 **OCA-B mutagenesis and co-IP.** For generation of the OCA-B double point mutant, a plasmid
582 transiently expressing human OCA-B, pCATCH-Bob.1[76], was sequentially mutagenized using
583 QuickChange (ThermoFisher). Correct mutagenesis and lack of additional mutations was confirmed by
584 resequencing. Protein expression was confirmed by transiently transfect HCT116 cells, which do not
585 express endogenous OCA-B. HCT116 lysate preparation, co-immunoprecipitation of OCA-B and
586 endogenous Jmjd1a, and immunoblot detection was performed using the same conditions as
587 described[4]. For co-IP using M12 cells, lysis buffer consisted of 50 mM Tris-Cl, pH 7.4, 150mM NaCl,
588 0.5%NP-40, 1 mM EDTA,1 mM EGTA, plus protease/phosphatase inhibitors (PhosSTOP, Roche).
589 Lysates were incubated with 2.5 µg Jmjd1A antibody (Bethyl) and protein-G Dynabeads
590 (ThermoFisher) in lysis buffer containing 20% glycerol overnight at 4°C. After overnight incubation,

591 the indicated concentrations of peptide or PBS vehicle was added and incubated for a further 3 hr at
592 4°C prior to bead precipitation and washing 3× in lysis buffer plus 20% glycerol. Co-precipitated
593 OCA-B was analyzed by SDS-PAGE and immunoblot.
594
595 **OCA-B inhibitor peptide synthesis.** Unique chemically synthesized peptide sequences were as
596 follows: Peptide#1, ARPYQGVRVKEPVK; Peptide#2/JumOCA, VKELLRRKRGH; Peptide#3,
597 ARPYQGVRVKEPVKELLRRKRGH; Scrambled peptide, VLREKGKRHLR. Peptides were
598 synthesized with and without a covalent C-terminal linker and Tat membrane-penetrating peptide
599 (GSG-GRKKRRQRRRGY). Fmoc protected amino acids were obtained from Protein Technologies
600 Inc. 1-[Bis(dimethylamino)methylene]-1H-1,2,3-triazolo[4,5-b]pyridinium 3-oxid
601 hexafluorophosphate (HATU) was purchased from Chemimpex Inc. H-Rink-Amide-ChemMatrix
602 (RAM) was purchased from Biotage. N,N-diisopropylethylamine (DIEA), dichloromethane (DCM),
603 triisopropylsilane (TIS) were purchased from Sigma Aldrich. Dimethylformamide (DMF),
604 trifluoroacetic acid (TFA), acetonitrile (ACN), and ethyl ether were purchased from Fisher Scientific.
605 Peptides were synthesized using automated Fmoc SPPS chemistry on synthesizer (Syro I). Briefly, 220
606 mg of RAM resin (Loading = 0.45 mmol/g) was swelled in DCM for 15 min and followed by adding in
607 a solution of specific Fmoc protected amino acid (AA = 0.1 mmol, DIEA = 0.2 mmol in DCM = 4 mL)
608 and incubated at room temperature for 1.5 h. Then the resin was washed with DMF and DCM and
609 incubated with 5 mL of DCM containing 16% v/v MeOH and 8% v/v DIEA for 5 min. This action was
610 repeated for 5 times before thoroughly washed with DCM and DMF. Then the resin was set to
611 synthesizer for automated synthesis. Coupling reactions were performed using HATU (5 eq.), DIPEA
612 (10 eq.) and amino acid (5 eq.) in DMF with 15 min heating to 70 oC (50 oC for Cys). Deprotection
613 reaction was performed using 20% (v/v) Piperidine in DMF, 5 min rt for 2 rounds. Peptides were
614 cleaved from the resin by treatment with a cocktail buffer (3 mL/0.1 mmol, TFA:H2O:TIS:EDT =
615 95:2:2:1) for 2.5 h. Peptide-TFA solution was then filtered and precipitated in cold ether, and
616 centrifuged and washed with ether twice and vacuum-dried. The crude product was then purified by
617 RP HPLC. Peptides characterization was performed by LC/MS on an Xbridge C18 5 µm (50 x 2.1
618 mm) column at 0.4 mL/min with a water/acetonitrile gradient in 0.1% formic acid on an Agilent 6120
619 Quadrupole LC/MS system. Fractions collected from HPLC runs were also analyzed by LC/MS. The
620 purified fractions containing the targeted product were collected and lyophilized using a Labconco
621 Freeze Dryer. All samples were analyzed by the following conditions: Preparative reverse phase HPLC
622 of crude peptides was performed on a Jupiter 5 µ C18 300 Å (250×10 mm) column at 3 mL/min with a
623 water/acetonitrile (ACN) gradient in 0.1% TFA on an Agilent 1260 HPLC system. Purity, isomer co-

624 injection and stability checks were performed on HPLC on Phenomenex Gemini C18 3 µm (110 Å
625 150×3 mm) column.
626
627 **OCA-B inhibitor peptide treatment.** Anesthetized pre-diabetic WT NOD females with glucose levels
628 newly-risen to between 225 to 275 mg/dL were treated with the inhibitor or control peptides by
629 intravenous (retro-orbital) injection, 3 times every 12 hr. Blood glucose levels were measured at every
630 injection. 4 hr after the last injection, pancreata and pancreatic lymph nodes (PLNs) were collected and
631 cell populations were analyzed by flow cytometry.
632
633 **Histology.** Formalin-fixed pancreatic tissues were embedded in paraffin. H&E-stained sections were
634 scored for islet inflammation based on published precedents[77]: 0, sparse surrounding sentinel
635 leukocytes, no insulitis; 1, peri-islet leukocytes; 2, some into islet, <50% of islet area; 3, islet insulitis
636 with >50% of islet area occupied by leukocytes; 4, islets destroyed with fibrotic remnants.
637
638 **Statistical analyses.** All error bars denote ±SEM. Two-tailed student T-tests were used to ascribe
639 statistical significance. For all figures, *=*p*-value ≤0.05; **=*p*-value ≤0.005.

Acknowledgements

We thank P. Santamaria, M. Williams, M. Bettini and F. Gounari for critical reading of the manuscript. We thank A. Chervonsky (U. Chicago) for the gift of NOD.Cre^{CD4} mice. We thank J. Marvin and the University of Utah Health Sciences Center Flow Cytometry Core facility for assistance with flow cytometry. We thank M. Hanson and the University of Utah Health Sciences DNA/peptide synthesis core. This work was supported by grants to DT from the Praespero Foundation, Juvenille Diabetes Research Foundation (1-INO-2018-647-A-N) and National Institutes of Health (R01-AI100873).

Author's contributions

DT conceived the study and designed experiments, supervised the study, and provided administrative, technical and material support. HK, AS, AI and JLJ acquired and interpreted the data. JP performed high-level analysis of scRNAseq and TCR clonotype data. CG helped generate critical reagents. BDE, DH-CC, XH and PJ provided material and intellectual support. All authors were involved in writing, reviewing and revising the manuscript.

654 **Figure legends**

655

656 **Fig. 1 | Loss of OCA-B protects NOD mice from T1D. a**, Targeting event. Crossing with FLP^{Rosa26}
657 results in conditional (*fl*) allele. Primer-pairs used for genotyping are depicted with arrows. **b**, Example
658 genotyping of the targeted allele and recombination events. Founder animal is in lane 2. The primer-
659 pairs shown in (a) were used. **c**, The *Ocab* (*Pou2af1*) conditional allele was crossed to Cre^{CD4}. Total
660 splenic $CD4^+$ T cells were isolated from an $Ocab^{fl/fl}Cre^{CD4}$ animal or a $Ocab^{+/fl}Cre^{CD4}$ littermate
661 control, and stimulated for 2 d in vitro using plate-bound CD3ε and soluble CD28 antibodies. An
662 OCA-B immunoblot of stimulated total T cells is shown. β-actin is shown as a loading control. **d**,
663 Kaplan-Meier plot of diabetes-free survival in littermate female NOD.$Ocab1^{fl/fl}Cre^{CD4}$ (n=12) and
664 NOD.$Ocab1^{fl/fl}$ (n=14) mice. Diabetes criterion was ≥250 mg/dL blood glucose. HR=hazard ratio. **e**,
665 Avearage blood glucose levels from mice shown in panel (c) is shown. **f**, Percent diabetes-free survival
666 in germline knockout NOD.$Ocab^{-/-}$ (n=16) and control NOD.$Ocab^{+/+}$ (n=17) mice were plotted based
667 blood glucose cutoff of ≥250 mg/dL.

668

669 **Fig. 2 | NOD.*Ocab* conditional mice have fewer islet IFNγ expressing CD8 T cells and**
670 **macrophages, and more Tregs compared to controls. a**, Pancreatic islet leukocytes were isolated
671 from 8 week- or 24 week-old littermate female NOD.$Ocab1^{fl/fl}Cre^{CD4}$ (8 week; n=3, 24 week; n=5) or
672 NOD.$Ocab1^{fl/fl}$ (8 week; n=3, 24 week; n=4) mice and analyzed by flow cytometry. Mean
673 $CD45^+CD11b^+F4/80^+$ cell frequencies are depicted. **b**, Frequencies of $CD45^+CD11b^+F4/80^+$ cells from
674 representative animals in panel (a) are shown. Plots were gated on $CD45^+$ cells. **c**, Mean percentages of
675 total pancreatic-infiltrating $CD8^+$ T cell in 12 week-old NOD.$Ocab1^{fl/fl}Cre^{CD4}$ or control
676 NOD.$Ocab1^{fl/fl}$ mice are plotted. Cells were independently purified from 3 pancreata and gated on
677 $CD45^+$. **d**, IFNγ expressing $CD8^+$ T cell percentages in 16 week old-NOD.$Ocab1^{fl/fl}Cre^{CD4}$ (n=3) and
678 littermate control islets (n=5) are shown. **e**, Percentages of FoxP3-expressing $CD4^+$ T cells in pre-
679 diabetic (8 week) NOD.*Ocab* conditional and control female mice are plotted. N=3 for each group.
680 Mean of results is shown. **f**, NOD.$Ocab^{fl/fl}$ or NOD.$Ocab^{fl/fl}Cre^{CD4}$ pups were treated with anti-CD25
681 antibodies intraperitoneally on day 10 and 17 after birth to deplete Tregs (red arrows). Mice were
682 monitored for T1D emergence as in Fig. 1.

683

684 **Fig. 3 | T cell conditional OCA-B loss reduces the numbers of activated, autoreactive pancreatic**
685 **islet T cells. a**, scRNAseq was performed using total islet $CD45^+$ cells from prediabetic

686 NOD.*Ocab*$^{fl/fl}$Cre^{CD4} or control NOD.*Ocab*$^{fl/fl}$ mice (n=3 for each group). Cell populations were plotted
687 using UMAP (Seurat R package) and percentages in each cluster are shown for each genotype.
688 Different populations were identified using Seurat R package function FindMarkers. **b**, Four
689 populations from panel (a) were analyzed for differential gene expression. Identified genes are shown
690 as a scatter plot. Significantly differentially expressed genes (adjusted *p*-value <0.05) are shown in red.
691 **c**, UMAP plots similar to (a) are shown, except cells expressing TCR clonotype 13-3 are shown. The
692 non-naïve (activated+memory) CD8$^+$ cell population identified in (a) is shown in red. **d**, Percent
693 contribution of the top 21 identified TCR clonotypes to total activated+memory CD8$^+$ cells is shown.
694 The V genes comprising the top 6 clonotypes are also shown. **e**, Cells positive for clonotypes 1-5 are
695 shown for two clusters, non-naïve (activated+memory) CD8$^+$ T cells and CTLA4$^+$FR4$^+$ anergic cells
696 (consisting of mostly CD4$^+$ cells). For each cluster, positive cells are shown in dark blue. An overlay
697 of control and OCA-B deficient cell populations is shown, however because each clonotype is only
698 observed in a single genotype (panel d), all cells can be mapped back entirely to OCA-B deficient or
699 control (clonotypes 1 and 4: OCA-B deficient; clonotypes 2, 3 and 5: control).
700
701 **Fig. 4 | OCA-B loss protects NOD mice from T1D in spontaneous and polyclonal splenocyte**
702 **transfer models but not in monoclonal transfer models. a**, 2×10^5 purified CD4$^+$CD25$^-$ splenic T
703 cells from NOD.BDC2.5.*Ocab*$^{-/-}$ or control NOD.BDC2.5.*Ocab*$^{+/+}$ donors were injected retro-orbitally
704 into NOD.Scid (n=6 for each group) mice. Diabetes-free survival (≥250 mg/dL) is shown. **b**, 1.5×10^6
705 purified splenic total CD4$^+$ T cells from NOD.BDC2.5.*Ocab*$^{-/-}$ or control donors were transferred into
706 NCG mice (n=5 for each group). Mice were monitored for diabetes development. **c**, Total NOD
707 splenocytes (5×10^6) from prediabetic 6- to 8-wk-old sex-matched NOD.*Ocab1*$^{fl/fl}$Cre^{CD4} or control
708 NOD.*Ocab1*$^{fl/fl}$ donors were adoptively transferred into sex-matched NOD.Scid (n=7 for each group)
709 recipients. Diabetes incidence rates are shown. **d**, At 13 weeks post-transfer, the proportion of IFNγ-
710 expressing CD8$^+$ T cells was assessed by flow cytometry in pancreata isolated from mice receiving
711 splenocytes from NOD.*Ocab1*$^{fl/fl}$Cre^{CD4} or NOD.*Ocab1*$^{fl/fl}$ donors in panel (c). **e**, Pancreata from the
712 same mice as in (d) were fixed, sectioned and H&E stained. Pathological scores are shown based on 6-
713 7 islets per slide, 3 slides per mouse and 3 mice in each group (>60 islets per group). **f**, Example
714 pancreatic images from endpoint animals. Yellow arrows indicate islet positions. Images were
715 collected at 10× magnification. **g**, The *Ocab* null allele was crossed to NY8.3 TCR transgenic mice.
716 Spontaneous T1D was measured in female *Ocab*$^{-/-}$ (n=20) or control *Ocab*$^{+/+}$ (n=12) littermates. **h**,
717 Naïve CD4$^+$ or CD8$^+$ T cells were isolated from C57BL/6 spleens and stimulated for up to two days in

718 vitro using anti-CD3ε and CD28 antibodies. Cells were then washed and replated in the presence of
719 exogenous IL-2. After 8 days rest in culture, cells were restimulated for 6 hr. Lysates were prepared
720 from each step and subjected to OCA-B immunoblotting to assess changes in expression. Oct1 and β-
721 actin are shown as controls.
722
723 **Fig. 5 | OCA-B loss in CD4$^+$ T cells increases anergy in vitro. a**, Naïve CD4$^+$ C57BL/6 T cells were
724 stimulated in vitro for 24 hr with anti-CD3ε antibodies ± co-stimulation with CD28 antibodies.
725 Lystates were prepared and subjected to immunoblotting using OCA-B antibodies. β-actin is shown as
726 a loading control. **b**, Naïve OCA-B deficient and control CD4$^+$ T cells were stimulated in vitro with
727 anti-CD3ε antibodies. 48 hr later, the cells were re-stimulated with PMA and ionomycin, and analyzed
728 by flow cytometry. Representative frequencies of cytokine expressing CD4$^+$ CD44$^+$ cells are shown. **c**,
729 Quantitation using independently purified cells from the spleens of 4 mice treated similar to (b). **d**,
730 OCA-B deficient and control CD4$^+$ T cells were stimulated in vitro with indicated antibodies, and
731 analyzed by flow cytometry. Mean of FR4^{hi} CD73^{hi} CD4$^+$ CD44$^+$ cell frequencies are shown using
732 independently purified cells from the spleens of 3 mice, with two technical culture replicates
733 performed for each mouse (n=6). **e**, Similar to panel (d), except frequencies of CD4$^+$CD44$^+$ICOS$^+$ cells
734 are plotted. **f**, Similar to panel (d), except average percentage of CD4$^+$CD44$^+$CD25$^+$ cells are plotted.
735
736 **Fig. 6 | Design and validation of OCA-B peptide inhibitors. a**, OCA-B N-terminus/Oct1 DNA
737 binding domain/octamer binding DNA co-crystal structure (PDB ID 1CQT)[48]. Gray: DNA. Green:
738 Oct1 DNA binding domain. Cyan: OCA-B. Structured OCA-B N- and C-termini (residues 16 and 38)
739 are labeled. Relevant OCA-B residues from panel (b) are highlighted. Red dashed line shows position
740 of the Oct1 linker domain. **b**, Top alignment of the human androgen receptor (AR) isoform transcript
741 variant 1 (Sequence ID: ADD26780.1) co-activator interaction domain (residues 698-721) with full-
742 length human Oct1 and OCA-B. The Oct1 linker domain and OCA-B N-terminus most resemble the
743 area of AR that interacts with Jmjd1a. Green serines: putative ERK phospho-acceptor sites. Yellow:
744 similar or identical amino acids. Asterisks: known human point mutations that block coactivator
745 binding and cause androgen insensitivity syndrome in humans. Pairwise alignments were performed
746 using the FASTA algorithm (https://embnet.vital-it.ch/software/LALIGN_form.html) and trimmed for
747 the 3-way overlap. **c**, Alignment of human and mouse primary OCA-B peptide sequences. **d**, Co-IP of
748 Jmjd1a with double point-mutant OCA-B and wild-type control. HCT116 cells (which lack
749 endogenous OCA-B) transfected with WT or mutant OCA-B constructs were used. Expression of

750 proteins was checked 48 hrs after transfection by Western blotting. 50 μg protein was loaded in each
751 lane. **e**, Indicated peptide sequences were synthesized as C-terminal Tat fusions for membrane
752 permeability. Arrows indicate position of mutant in (b) and (d). **f**, *Il2* mRNA expression in primary
753 $CD4^+$ T cells treated with 50 μM JumOCA peptide was measured relative to β-actin internal standard
754 by RT-qPCR. Cells were stimulated with CD3ε/CD28 antibodies for two days, rested for a further 8
755 days in the presence of exogenous recombinant IL-2, and restimulated for a further 6 hr. Peptide was
756 included during resting and restimulation only, and replaced every other day with media changes. **g**,
757 IL-2 cytokine expression in primary $CD4^+$ T cells cultured with 50μM peptide at initial treatment, and
758 with 25μM peptide from the secondary treatment was measured by flow cytometry. Cells were treated
759 similarly to (f) except collection, brefeldin A treatment and processing for flow cytometry occurred 24
760 hr post-restimulation. **h**, $CD4^+CD44^+IL2^+$ T cell frequencies from representative samples in panel (g)
761 are shown. Plots were gated on CD4 and CD44. **i**, The interaction between OCA-B and Jmjd1a was
762 measured in a co-immunoprecipitation assay. After incubation with protein-G beads, 0.2 μg/μL control
763 scambled (Scram) or double point mutant (DM) peptide, or JumOCA peptide, were added for a further
764 3 hr prior to precipitation and washing. 1% input (lane 1) is shown as a control.
765
766 **Fig. 7 | OCA-B inhibitor peptide injections protect NOD mice from newly-arisen diabetes. a**, 3
767 doses of 10 mg/kg OCA-B inhibitor peptide (n=4) or control peptide (n=5) were injected retro-orbitally
768 every 12 hr into 12-18 week-old NOD female littermate mice whose glucose levels were newly-risen
769 above 225 mg/dL but still below 275 mg/dL. Glucose levels of peptide injected mice are shown right
770 before each injection, and 12 hr after final injection. Control peptide=Tat alone. **b**, 4hr after the last
771 injection of peptides in panel (a), PLN $CD4^+$ and $CD8^+$ T cell percentages were analyzed by flow
772 cytometry. **c**, Mean of islet IL-17 expressing T cells in the same mice as in (b) were analyzed by flow
773 cytometry and plotted. **d**, Similar analysis as (c) except for IFNγ.
774

775 **References**

776 1. Lernmark, A. & Larsson, H.E. Immune therapy in type 1 diabetes mellitus. *Nat Rev Endocrinol* **9**, 92-
777 103 (2013).

778 2. Cooke, D.W. & Plotnick, L. Type 1 diabetes mellitus in pediatrics. *Pediatr Rev* **29**, 374-384; quiz 385
779 (2008).

780 3. Staeva, T.P., Chatenoud, L., Insel, R. & Atkinson, M.A. Recent lessons learned from prevention and
781 recent-onset type 1 diabetes immunotherapy trials. *Diabetes* **62**, 9-17 (2013).

782 4. Shakya, A. *et al.* Oct1 and OCA-B are selectively required for CD4 memory T cell function. *J Exp Med*
783 **212**, 2115-2131 (2015).

784 5. Kim, H. *et al.* T cell-selective deletion of Oct1 protects animals from autoimmune neuroinflammation
785 while maintaining neurotropic pathogen response. *J Neuroinflammation* **16**, 133 (2019).

786 6. Shakya, A., Kang, J., Chumley, J., Williams, M.A. & Tantin, D. Oct1 is a switchable, bipotential
787 stabilizer of repressed and inducible transcriptional states. *The Journal of biological chemistry* **286**, 450-
788 459 (2011).

789 7. Yosef, N. *et al.* Dynamic regulatory network controlling TH17 cell differentiation. *Nature* **496**, 461-468
790 (2013).

791 8. van Heel, D.A. *et al.* Inflammatory bowel disease is associated with a TNF polymorphism that affects
792 an interaction between the OCT1 and NF(-kappa)B transcription factors. *Hum Mol Genet* **11**, 1281-1289
793 (2002).

794 9. Vince, N. *et al.* HLA-C Level Is Regulated by a Polymorphic Oct1 Binding Site in the HLA-C Promoter
795 Region. *Am J Hum Genet* **99**, 1353-1358 (2016).

796 10. Cunninghame Graham, D.S., Wong, A.K., McHugh, N.J., Whittaker, J.C. & Vyse, T.J. Evidence for
797 unique association signals in SLE at the CD28-CTLA4-ICOS locus in a family-based study. *Hum Mol*
798 *Genet* **15**, 3195-3205 (2006).

799 11. Kiesler, P., Shakya, A., Tantin, D. & Vercelli, D. An allergy-associated polymorphism in a novel
800 regulatory element enhances IL13 expression. *Hum Mol Genet* **18**, 4513-4520 (2009).

801 12. Farh, K.K. *et al.* Genetic and epigenetic fine mapping of causal autoimmune disease variants. *Nature*
802 **518**, 337-343 (2015).

803 13. Maurano, M.T. *et al.* Systematic localization of common disease-associated variation in regulatory
804 DNA. *Science* **337**, 1190-1195 (2012).

805 14. Leon Rodriguez, D.A., Carmona, F.D., Echeverria, L.E., Gonzalez, C.I. & Martin, J. IL18 Gene
806 Variants Influence the Susceptibility to Chagas Disease. *PLoS Negl Trop Dis* **10**, e0004583 (2016).

807 15. Games Collaborative, G. *et al.* Linkage disequilibrium screening for multiple sclerosis implicates JAG1
808 and POU2AF1 as susceptibility genes in Europeans. *J Neuroimmunol* **179**, 108-116 (2006).

809 16. Nakamura, M. *et al.* Genome-wide association study identifies TNFSF15 and POU2AF1 as
810 susceptibility loci for primary biliary cirrhosis in the Japanese population. *Am J Hum Genet* **91**, 721-728
811 (2012).

812 17. Serreze, D.V. *et al.* B lymphocytes are essential for the initiation of T cell-mediated autoimmune
813 diabetes: analysis of a new "speed congenic" stock of NOD.Ig mu null mice. *J Exp Med* **184**, 2049-2053
814 (1996).

815 18. Hattori, M. *et al.* The NOD mouse: recessive diabetogenic gene in the major histocompatibility
816 complex. *Science* **231**, 733-735 (1986).

817 19. Serreze, D.V. *et al.* Subcongenic analysis of the Idd13 locus in NOD/Lt mice: evidence for several
818 susceptibility genes including a possible diabetogenic role for beta 2-microglobulin. *J Immunol* **160**,
819 1472-1478 (1998).

820 20. Kim, U. *et al.* The B-cell-specific transcription coactivator OCA-B/OBF-1/Bob-1 is essential for normal
821 production of immunoglobulin isotypes. *Nature* **383**, 542-547 (1996).

822 21. Wong, C.P., Li, L., Frelinger, J.A. & Tisch, R. Early autoimmune destruction of islet grafts is associated
823 with a restricted repertoire of IGRP-specific CD8+ T cells in diabetic nonobese diabetic mice. *J*
824 *Immunol* **176**, 1637-1644 (2006).

825 22. Makino, S., Muraoka, Y., Kishimoto, Y. & Hayashi, Y. Genetic analysis for insulitis in NOD mice.
826 *Jikken Dobutsu* **34**, 425-431 (1985).

827 23. Rosmalen, J.G. *et al.* Subsets of macrophages and dendritic cells in nonobese diabetic mouse pancreatic
828 inflammatory infiltrates: correlation with the development of diabetes. *Lab Invest* **80**, 23-30 (2000).

829 24. Peterson, J.D., Berg, R., Piganelli, J.D., Poulin, M. & Haskins, K. Analysis of leukocytes recruited to
830 the pancreas by diabetogenic T cell clones. *Cell Immunol* **189**, 92-98 (1998).

831 25. Cantor, J. & Haskins, K. Recruitment and activation of macrophages by pathogenic CD4 T cells in type
832 1 diabetes: evidence for involvement of CCR8 and CCL1. *J Immunol* **179**, 5760-5767 (2007).

833 26. Schloot, N.C. *et al.* Serum IFN-gamma and IL-10 levels are associated with disease progression in non-
834 obese diabetic mice. *Diabetes Metab Res Rev* **18**, 64-70 (2002).

835 27. Newby, B.N. *et al.* Type 1 Interferons Potentiate Human CD8(+) T-Cell Cytotoxicity Through a
836 STAT4- and Granzyme B-Dependent Pathway. *Diabetes* **66**, 3061-3071 (2017).

837 28. Krishnamurthy, B. *et al.* Autoimmunity to both proinsulin and IGRP is required for diabetes in
838 nonobese diabetic 8.3 TCR transgenic mice. *J Immunol* **180**, 4458-4464 (2008).

839 29. Wang, B. *et al.* Interferon-gamma impacts at multiple points during the progression of autoimmune
840 diabetes. *Proc Natl Acad Sci U S A* **94**, 13844-13849 (1997).

841 30. Brode, S., Raine, T., Zaccone, P. & Cooke, A. Cyclophosphamide-induced type-1 diabetes in the NOD
842 mouse is associated with a reduction of CD4+CD25+Foxp3+ regulatory T cells. *J Immunol* **177**, 6603-
843 6612 (2006).

844 31. Jaeckel, E., von Boehmer, H. & Manns, M.P. Antigen-specific FoxP3-transduced T-cells can control
845 established type 1 diabetes. *Diabetes* **54**, 306-310 (2005).

846 32. Mellanby, R.J., Thomas, D., Phillips, J.M. & Cooke, A. Diabetes in non-obese diabetic mice is not
847 associated with quantitative changes in CD4+ CD25+ Foxp3+ regulatory T cells. *Immunology* **121**, 15-
848 28 (2007).

849 33. Li, L. *et al.* beta cell-specific CD4+ T cell clonotypes in peripheral blood and the pancreatic islets are
850 distinct. *J Immunol* **183**, 7585-7591 (2009).

851 34. Berry, G. & Waldner, H. Accelerated type 1 diabetes induction in mice by adoptive transfer of
852 diabetogenic CD4+ T cells. *J Vis Exp*, e50389 (2013).

853 35. Presa, M. *et al.* The Presence and Preferential Activation of Regulatory T Cells Diminish Adoptive
854 Transfer of Autoimmune Diabetes by Polyclonal Nonobese Diabetic (NOD) T Cell Effectors into NSG
855 versus NOD-scid Mice. *J Immunol* **195**, 3011-3019 (2015).

856 36. Van Belle, T.L., Taylor, P. & von Herrath, M.G. Mouse Models for Type 1 Diabetes. *Drug Discov*
857 *Today Dis Models* **6**, 41-45 (2009).

858 37. Kurts, C. *et al.* CD4+ T cell help impairs CD8+ T cell deletion induced by cross-presentation of self-
859 antigens and favors autoimmunity. *J Exp Med* **186**, 2057-2062 (1997).

860 38. Verdaguer, J. *et al.* Spontaneous autoimmune diabetes in monoclonal T cell nonobese diabetic mice. *J*
861 *Exp Med* **186**, 1663-1676 (1997).

862 39. Kalekar, L.A. *et al.* CD4(+) T cell anergy prevents autoimmunity and generates regulatory T cell
863 precursors. *Nat Immunol* **17**, 304-314 (2016).

864 40. Vanasek, T.L., Khoruts, A., Zell, T. & Mueller, D.L. Antagonistic roles for CTLA-4 and the
865 mammalian target of rapamycin in the regulation of clonal anergy: enhanced cell cycle progression
866 promotes recall antigen responsiveness. *J Immunol* **167**, 5636-5644 (2001).

867 41. Kearney, E.R., Pape, K.A., Loh, D.Y. & Jenkins, M.K. Visualization of peptide-specific T cell
868 immunity and peripheral tolerance induction in vivo. *Immunity* **1**, 327-339 (1994).

869 42. Chai, J.G. & Lechler, R.I. Immobilized anti-CD3 mAb induces anergy in murine naive and memory
870 CD4+ T cells in vitro. *Int Immunol* **9**, 935-944 (1997).

871 43. Tuettenberg, A. *et al.* The role of ICOS in directing T cell responses: ICOS-dependent induction of T
872 cell anergy by tolerogenic dendritic cells. *J Immunol* **182**, 3349-3356 (2009).

873 44. Dong, C. & Nurieva, R.I. Regulation of immune and autoimmune responses by ICOS. *J Autoimmun* **21**,
874 255-260 (2003).

875 45. Dong, C. *et al.* ICOS co-stimulatory receptor is essential for T-cell activation and function. *Nature* **409**,
876 97-101 (2001).

877 46. Martinez, R.J. *et al.* Arthritogenic self-reactive CD4+ T cells acquire an FR4hiCD73hi anergic state in
878 the presence of Foxp3+ regulatory T cells. *J Immunol* **188**, 170-181 (2012).

879 47. Skwarczynska, M. & Ottmann, C. Protein-protein interactions as drug targets. *Future Med Chem* **7**,
880 2195-2219 (2015).

881 48. Green, D.R. A BH3 Mimetic for Killing Cancer Cells. *Cell* **165**, 1560 (2016).

882 49. Polo, J.M. *et al.* Specific peptide interference reveals BCL6 transcriptional and oncogenic mechanisms
883 in B-cell lymphoma cells. *Nat Med* **10**, 1329-1335 (2004).

884 50. Chasman, D., Cepek, K., Sharp, P.A. & Pabo, C.O. Crystal structure of an OCA-B peptide bound to an
885 Oct-1 POU domain/octamer DNA complex: specific recognition of a protein-DNA interface. *Genes Dev*
886 **13**, 2650-2657 (1999).

887 51. Klemm, J.D., Rould, M.A., Aurora, R., Herr, W. & Pabo, C.O. Crystal structure of the Oct-1 POU
888 domain bound to an octamer site: DNA recognition with tethered DNA-binding modules. *Cell* **77**, 21-32
889 (1994).

890 52. Gstaiger, M., Georgiev, O., van Leeuwen, H., van der Vliet, P. & Schaffner, W. The B cell coactivator
891 Bob1 shows DNA sequence-dependent complex formation with Oct-1/Oct-2 factors, leading to
892 differential promoter activation. *EMBO J* **15**, 2781-2790 (1996).

893 53. Yamane, K. *et al.* JHDM2A, a JmjC-containing H3K9 demethylase, facilitates transcription activation
894 by androgen receptor. *Cell* **125**, 483-495 (2006).

895 54. Thin, T.H. *et al.* Mutations in the helix 3 region of the androgen receptor abrogate ARA70 promotion of
896 17beta-estradiol-induced androgen receptor transactivation. *The Journal of biological chemistry* **277**,
897 36499-36508 (2002).

898 55. Schwarze, S.R., Hruska, K.A. & Dowdy, S.F. Protein transduction: unrestricted delivery into all cells?
899 *Trends Cell Biol* **10**, 290-295 (2000).

900 56. Caron, N.J., Quenneville, S.P. & Tremblay, J.P. Endosome disruption enhances the functional nuclear
901 delivery of Tat-fusion proteins. *Biochem Biophys Res Commun* **319**, 12-20 (2004).

902 57. Krautwald, S., Ziegler, E., Tiede, K., Pust, R. & Kunzendorf, U. Transduction of the TAT-FLIP fusion
903 protein results in transient resistance to Fas-induced apoptosis in vivo. *The Journal of biological*
904 *chemistry* **279**, 44005-44011 (2004).

905 58. Shi, W. *et al.* Transcriptional profiling of mouse B cell terminal differentiation defines a signature for
906 antibody-secreting plasma cells. *Nat Immunol* **16**, 663-673 (2015).

907 59. Kawakami, N. *et al.* Autoimmune CD4+ T cell memory: lifelong persistence of encephalitogenic T cell
908 clones in healthy immune repertoires. *J Immunol* **175**, 69-81 (2005).

909 60. Yeo, L. *et al.* Autoreactive T effector memory differentiation mirrors beta cell function in type 1
910 diabetes. *J Clin Invest* **128**, 3460-3474 (2018).

911 61. Chee, J. *et al.* Effector-memory T cells develop in islets and report islet pathology in type 1 diabetes. *J*
912 *Immunol* **192**, 572-580 (2014).

913 62. Parker, M.J. *et al.* Immune depletion with cellular mobilization imparts immunoregulation and reverses
914 autoimmune diabetes in nonobese diabetic mice. *Diabetes* **58**, 2277-2284 (2009).

915 63. Ikegami, I., Takaki, H., Kamiya, S., Kamekura, R. & Ichimiya, S. Bob1 enhances RORgammat-
916 mediated IL-17A expression in Th17cells through interaction with RORgammat. *Biochem Biophys Res*
917 *Commun* **514**, 1167-1171 (2019).

918 64. Chevrier, S., Kratina, T., Emslie, D., Karnowski, A. & Corcoran, L.M. Germinal center-independent,
919 IgM-mediated autoimmunity in sanroque mice lacking Obf1. *Immunol Cell Biol* **92**, 12-19 (2014).

920 65. Casellas, R. *et al.* OcaB is required for normal transcription and V(D)J recombination of a subset of
921 immunoglobulin kappa genes. *Cell* **110**, 575-585 (2002).

922 66. Citro, A. *et al.* CXCR1/2 inhibition blocks and reverses type 1 diabetes in mice. *Diabetes* **64**, 1329-1340
923 (2015).

924 67. Diana, J. & Lehuen, A. Macrophages and beta-cells are responsible for CXCR2-mediated neutrophil
925 infiltration of the pancreas during autoimmune diabetes. *EMBO Mol Med* **6**, 1090-1104 (2014).

926 68. Haskins, K. Pathogenic T-cell clones in autoimmune diabetes: more lessons from the NOD mouse. *Adv*
927 *Immunol* **87**, 123-162 (2005).

928 69. Kurts, C. *et al.* Constitutive class I-restricted exogenous presentation of self antigens in vivo. *J Exp Med*
929 **184**, 923-930 (1996).

930 70. Katz, J.D., Wang, B., Haskins, K., Benoist, C. & Mathis, D. Following a diabetogenic T cell from
931 genesis through pathogenesis. *Cell* **74**, 1089-1100 (1993).

932 71. Delong, T. *et al.* Pathogenic CD4 T cells in type 1 diabetes recognize epitopes formed by peptide
933 fusion. *Science* **351**, 711-714 (2016).

934 72. Zuber, J. *et al.* RNAi screen identifies Brd4 as a therapeutic target in acute myeloid leukaemia. *Nature*
935 **478**, 524-528 (2011).

936 73. Zwilling, S., Dieckmann, A., Pfisterer, P., Angel, P. & Wirth, T. Inducible expression and
937 phosphorylation of coactivator BOB.1/OBF.1 in T cells. *Science* **277**, 221-225 (1997).

938 74. Testa, G. *et al.* A reliable lacZ expression reporter cassette for multipurpose, knockout-first alleles.
939 *Genesis* **38**, 151-158 (2004).

940 75. Sitrin, J., Ring, A., Garcia, K.C., Benoist, C. & Mathis, D. Regulatory T cells control NK cells in an
941 insulitic lesion by depriving them of IL-2. *J Exp Med* **210**, 1153-1165 (2013).

942 76. Gstaiger, M., Knoepfel, L., Georgiev, O., Schaffner, W. & Hovens, C.M. A B-cell coactivator of
943 octamer-binding transcription factors. *Nature* **373**, 360-362 (1995).

944 77. Zhang, C. *et al.* Elimination of insulitis and augmentation of islet beta cell regeneration via induction of
945 chimerism in overtly diabetic NOD mice. *Proc Natl Acad Sci U S A* **104**, 2337-2342 (2007).

946

947

Kim et al. Figure 1

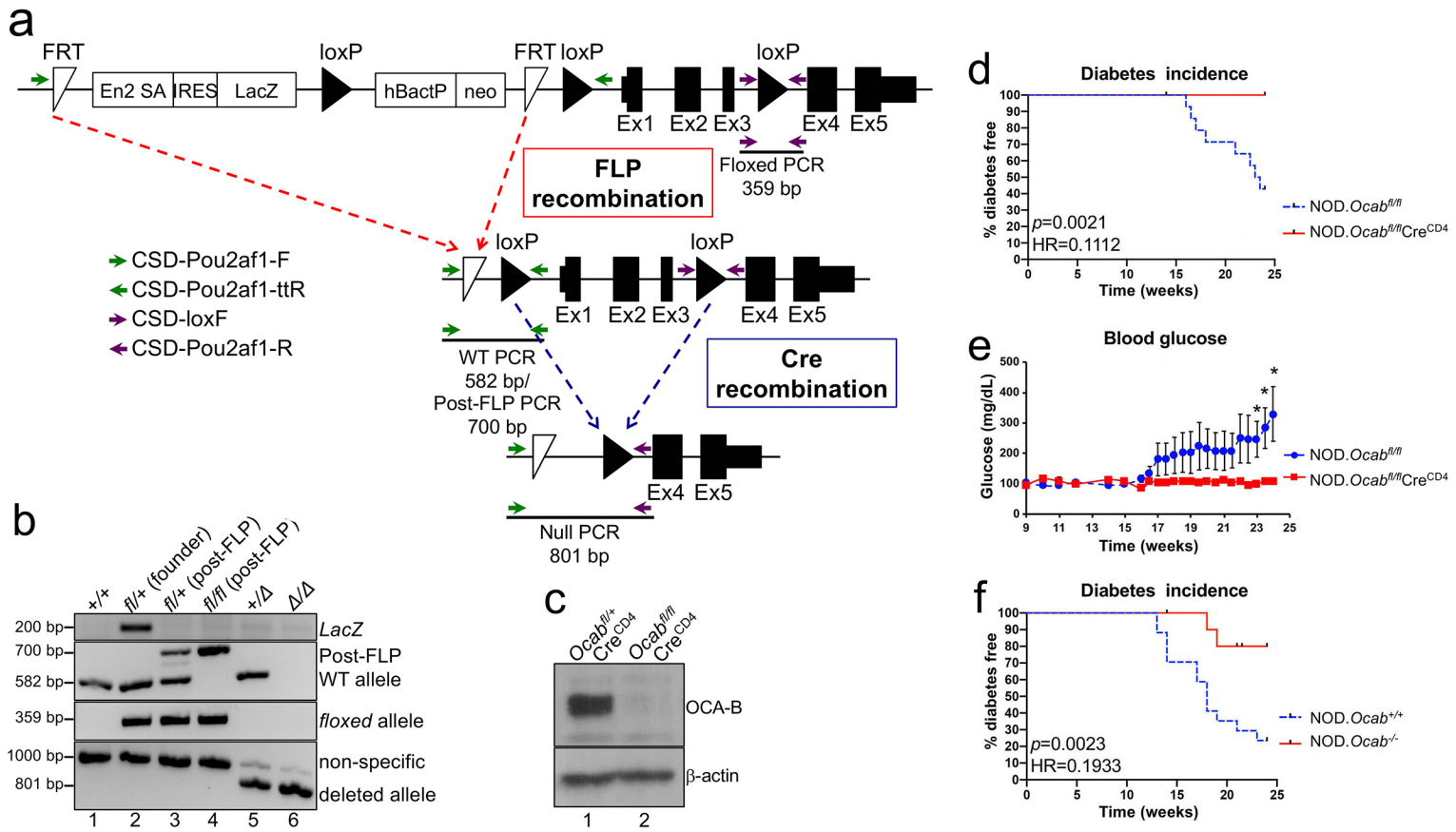

Kim et al. Figure 2

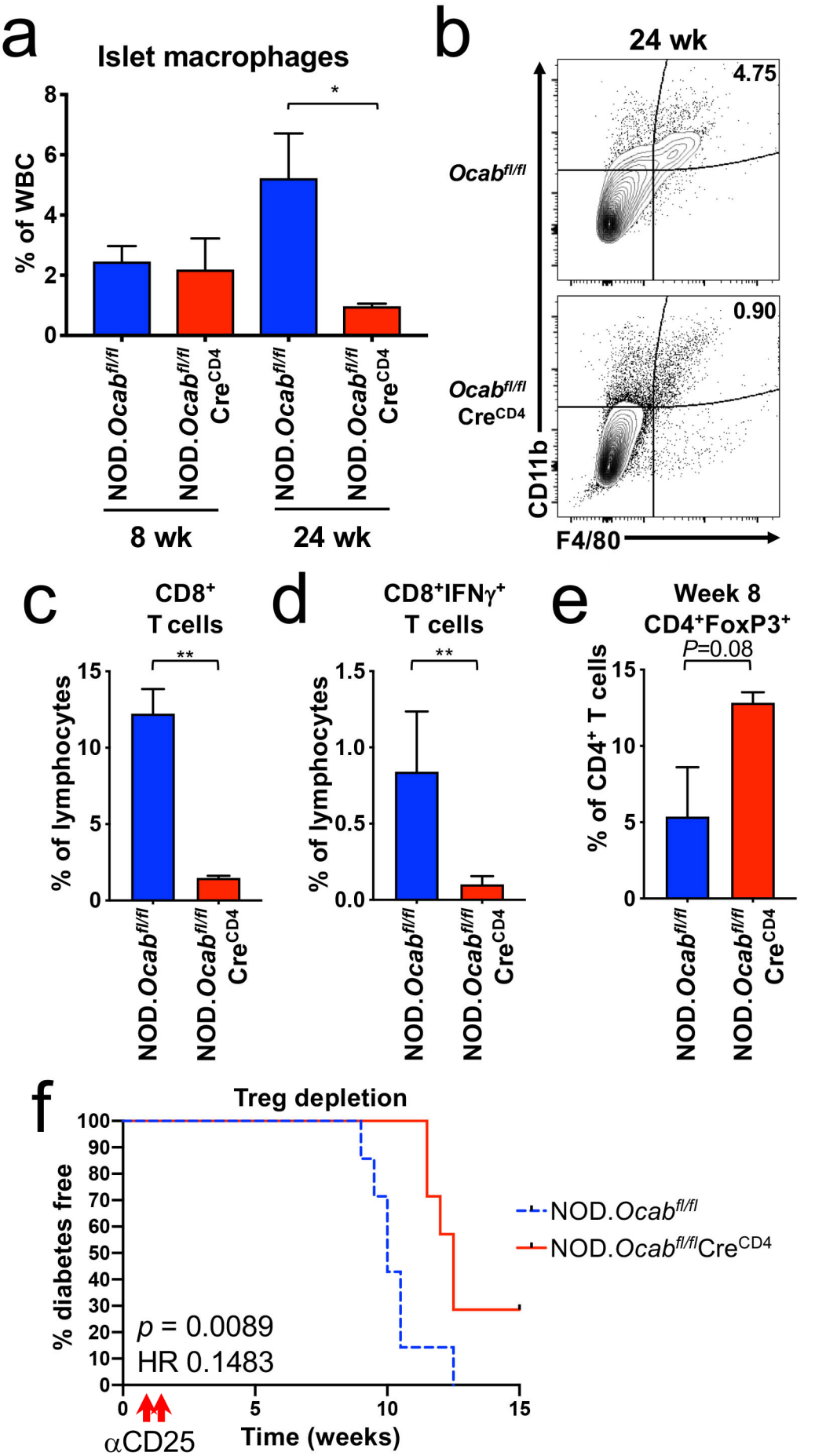

Kim et al. Figure 3

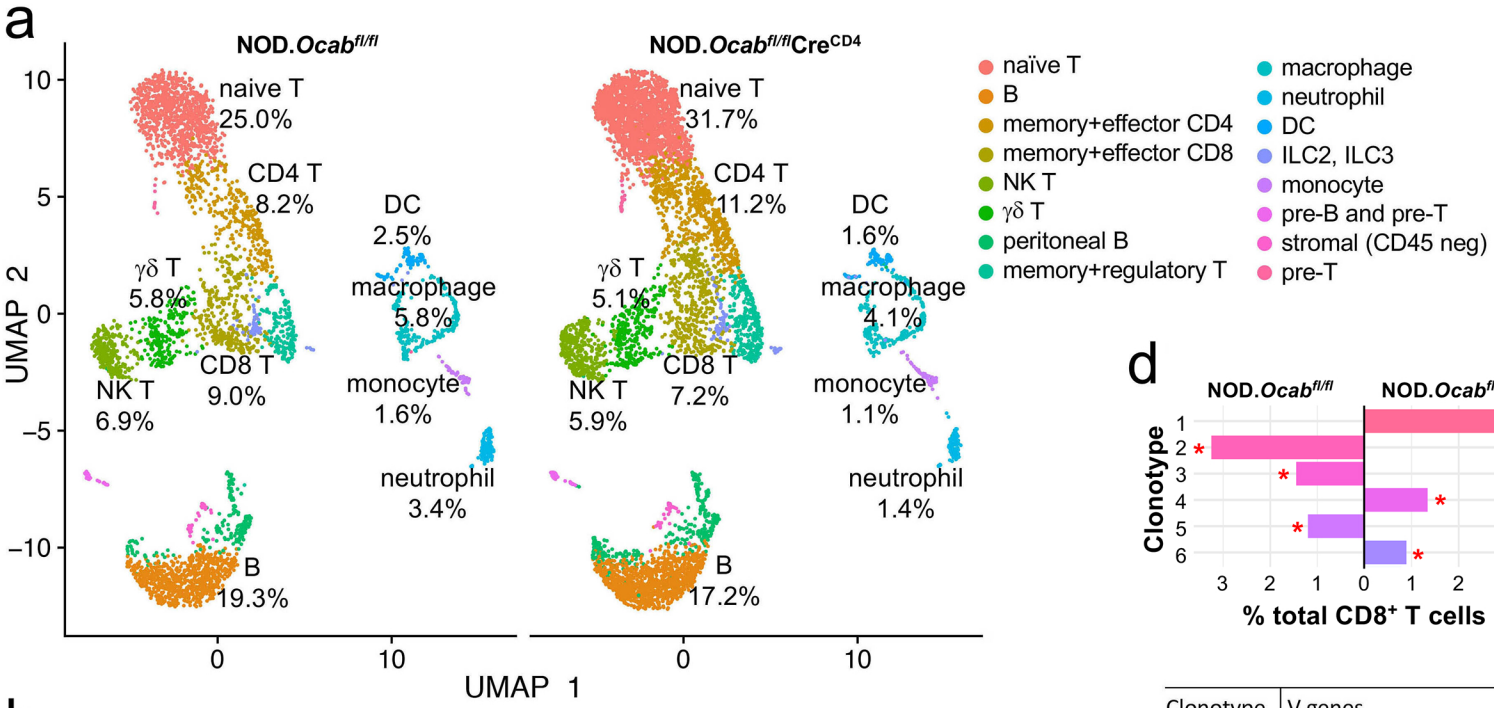

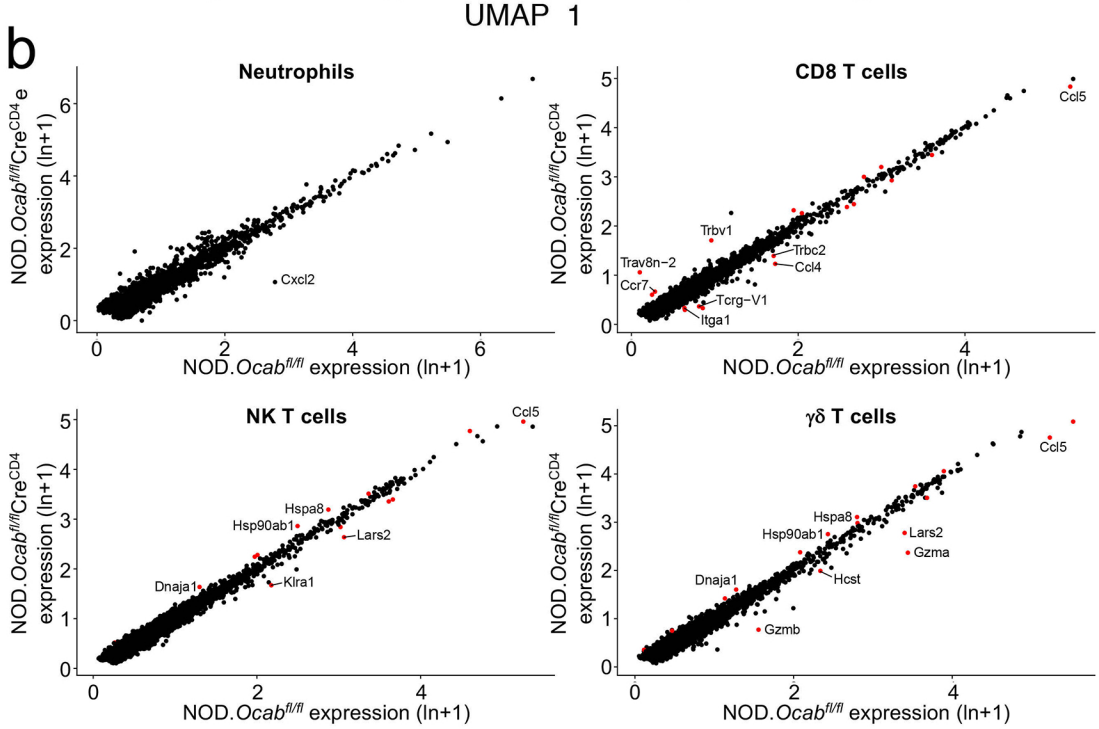

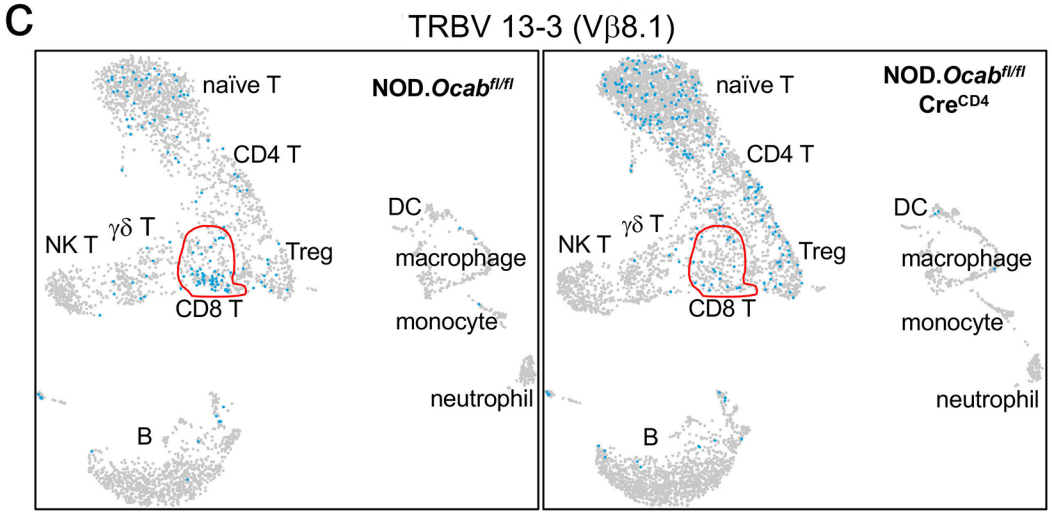

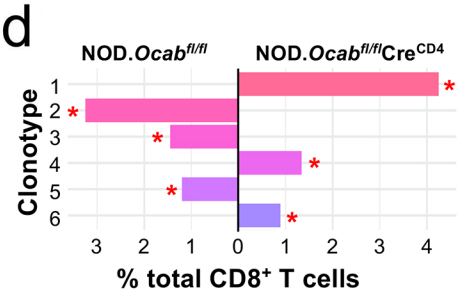

Clonotype	V genes
1	TRAV8N-2;TRBV1;TRBV15
2	TRAV16N;TRBV13-3
3	TRAV9-1;TRBV3
4	TRAV13-1;TRAV16N;TRBV15
5	TRBV13-3

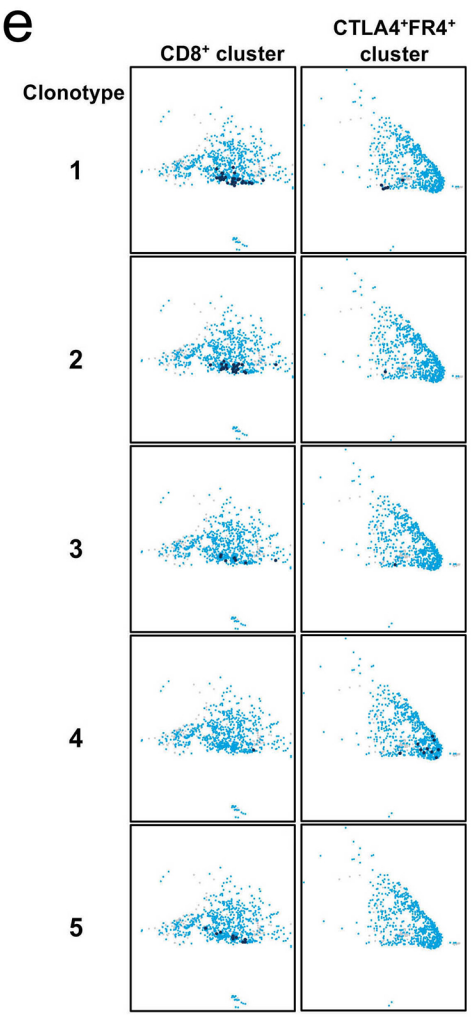

Kim et al. Figure 4

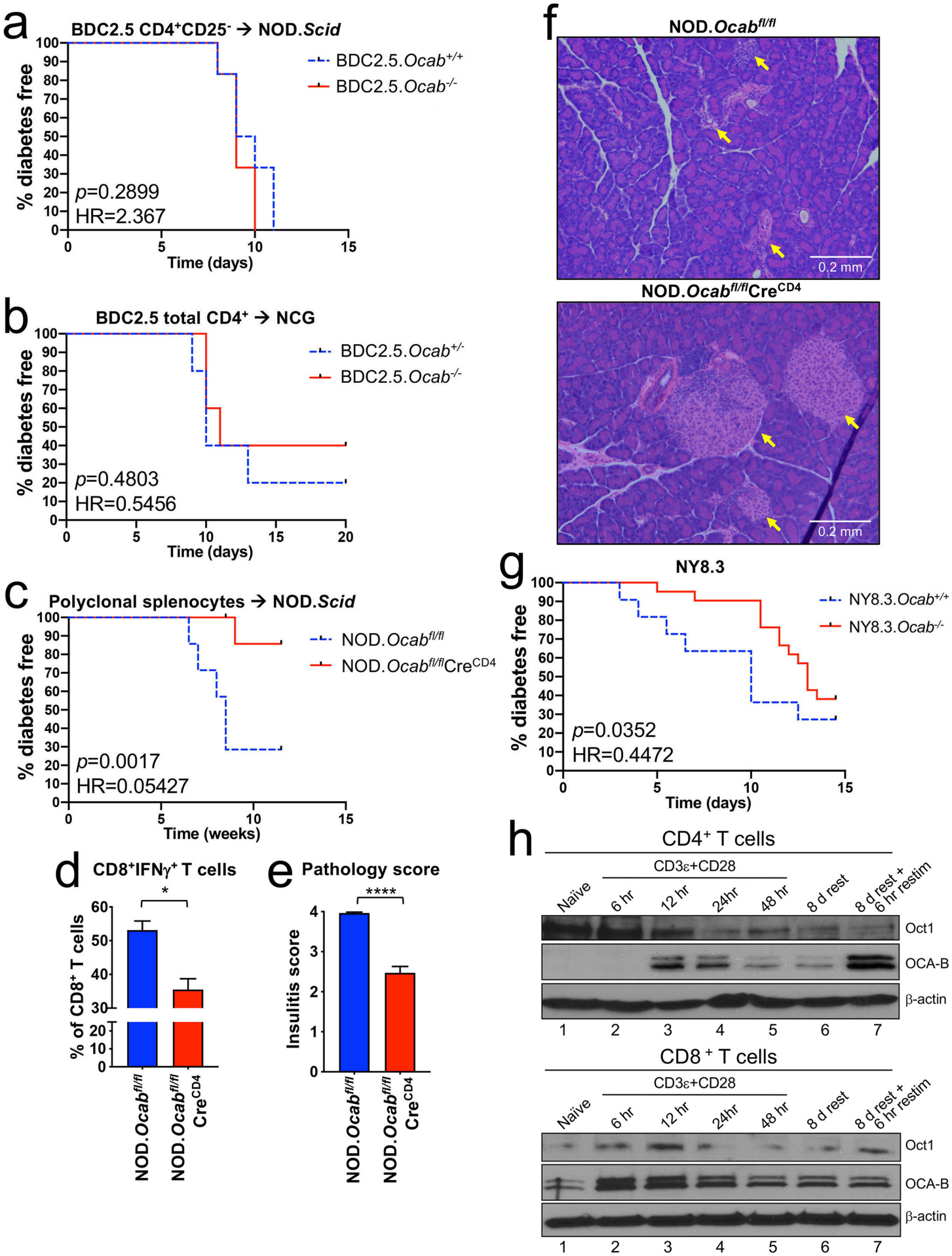

Kim et al. Figure 5

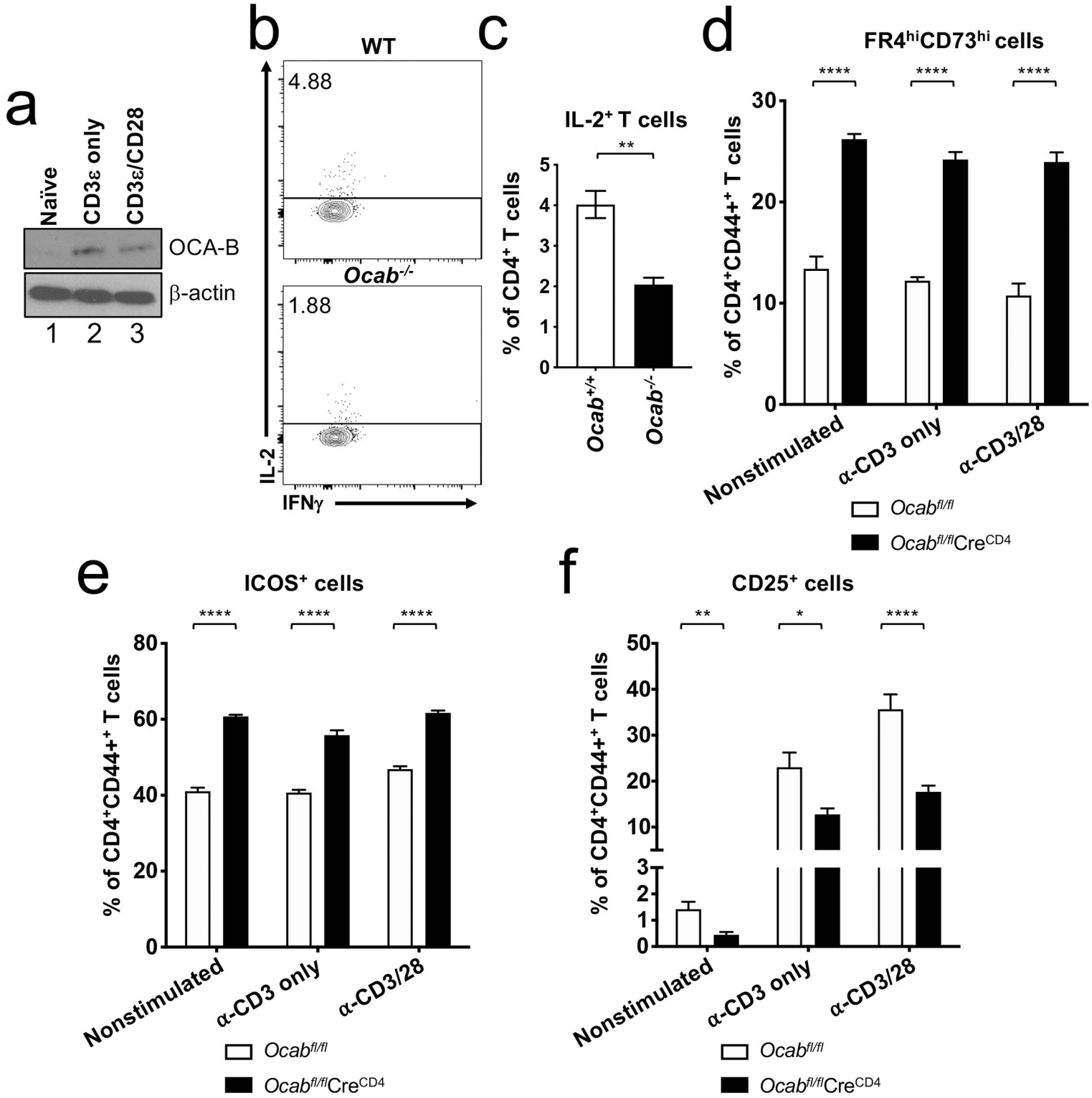

Kim et al. Figure 6

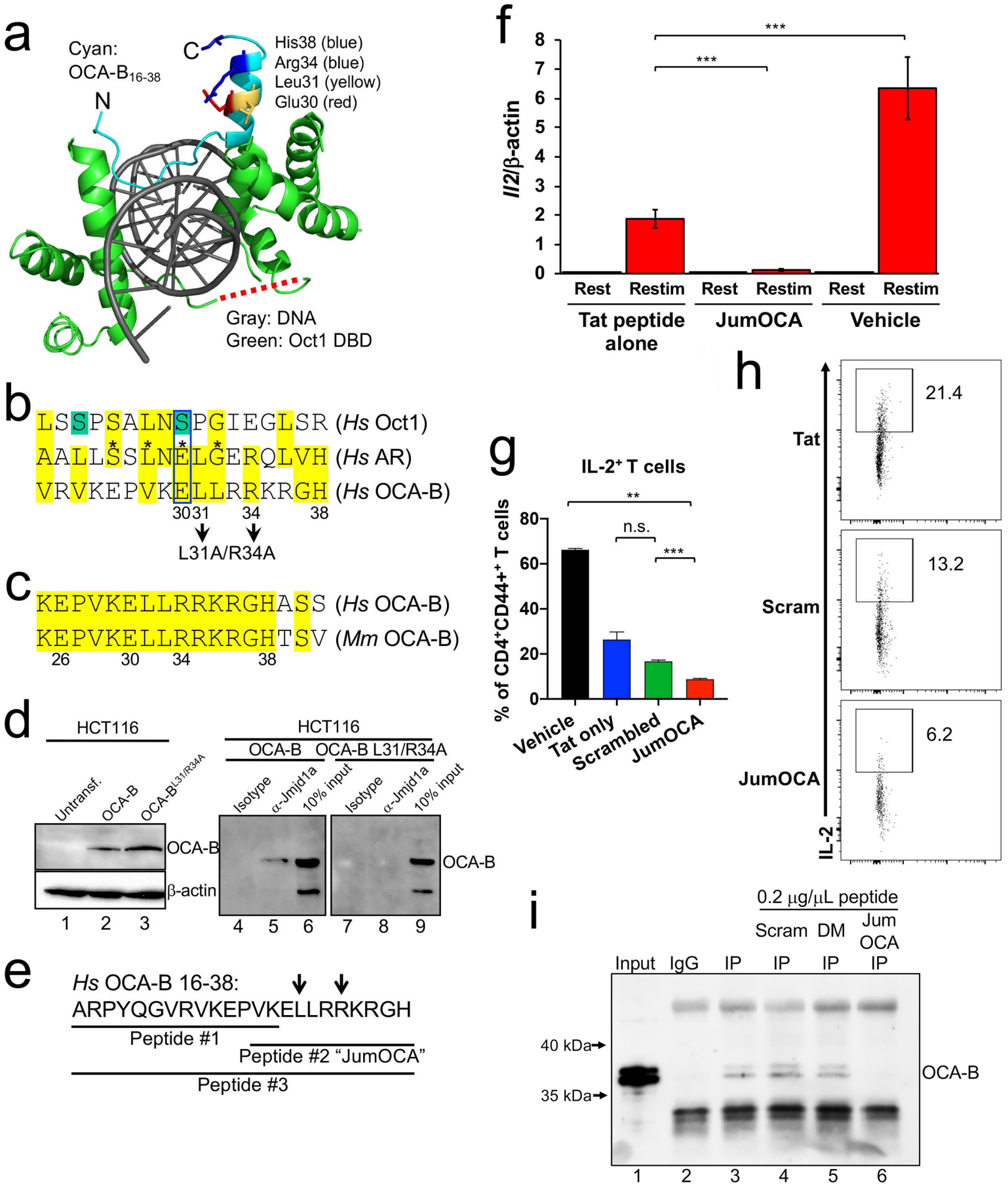
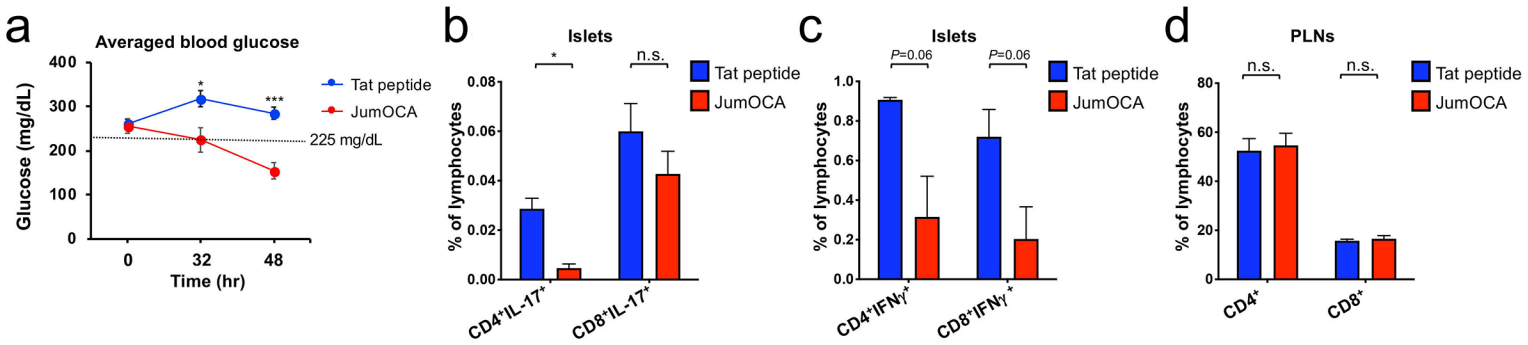
Kim et al. Figure 7